

Wild refitting for black box prediction

Martin J. Wainwright

Laboratory for Information and Decision Systems
 Statistics and Data Science Center
 EECS and Mathematics
 Massachusetts Institute of Technology

June 26, 2025

Abstract

We describe and analyze a computationally efficient refitting procedure for computing high-probability upper bounds on the instance-wise mean-squared prediction error of penalized non-parametric estimates based on least-squares minimization. Requiring only a single dataset and black box access to the prediction method, it consists of three steps: computing suitable residuals, symmetrizing and scaling them with a pre-factor ρ , and using them to define and solve a modified prediction problem recentered at the current estimate. We refer to it as wild refitting, since it uses Rademacher residual symmetrization as in a wild bootstrap variant. Under relatively mild conditions allowing for noise heterogeneity, we establish a high probability guarantee on its performance, showing that the wild refit with a suitably chosen wild noise scale ρ gives an upper bound on prediction error. This theoretical analysis provides guidance into the design of such procedures, including how the residuals should be formed, the amount of noise rescaling in the wild sub-problem needed for upper bounds, and the local stability properties of the block-box procedure. We illustrate the applicability of this procedure to various problems, including non-rigid structure-from-motion recovery with structured matrix penalties; plug-and-play image restoration with deep neural network priors; and randomized sketching with kernel methods.

1 Introduction

Prediction problems are ubiquitous throughout science and engineering. They are defined by a feature vector or covariate $X \in \mathcal{X}$ and a scalar response $Y \in \mathbb{R}$, and the goal is to determine a function $x \mapsto \hat{f}(x)$ that is a “good approximation” to y in a certain sense. When the quality of an estimate is measured by its mean-squared error, then it is a classical fact that the best predictor is given by the regression function $f^*(x) = \mathbb{E}[Y | X = x]$. The quality of a given estimate \hat{f} can then be measured by its mean-squared error or risk $\bar{\mathcal{R}}(\hat{f}) := \mathbb{E}_{X,Y}[(Y - \hat{f}(X))^2]$, or its excess risk

$$\bar{\mathcal{E}}(\hat{f}) := \underbrace{\mathbb{E}_{X,Y}[(Y - \hat{f}(X))^2]}_{\bar{\mathcal{R}}(\hat{f})} - \mathbb{E}_{X,Y}[(Y - f^*(X))^2]. \quad (1)$$

Here the expectations are taken over a future sample (X, Y) , independent of any training data used to produce \hat{f} . Since f^* is the optimal predictor in the mean-squared sense, the excess risk is always non-negative.

1.1 Methods for risk estimation

Given a predictor \hat{f} that has been fit on some training data, an important problem in practice is to estimate the excess risk $\bar{\mathcal{E}}(\hat{f})$, or simply the risk $\bar{\mathcal{R}}(\hat{f})$ itself. Given its importance, this

problem has been intensively studied, with a variety of approaches available. The simplest and most classical approach is the *hold-out method*; we split the original dataset into two separate pieces, and use the first piece to fit the estimate \hat{f} , and the second piece to obtain an unbiased estimate of the risk $\bar{\mathcal{R}}(\hat{f})$. However, the hold-out approach suffers from a number of deficiencies, notably its wastefulness in data use. A more sophisticated approach, dating back to the classic papers [23, 10], is cross-validation; see the paper [2] for a modern overview. Cross-validation involves repeated splitting of the dataset into parts used for training and testing; in this way, it avoids the wasteful use of data associated with the hold-out method. On the flip side, it is significantly more computationally expensive; for example, roughly speaking, a CV approach based on k -splits will require k -times more computation than hold-out. Note that hold-out and cross-validation apply to i.i.d. datasets¹, so that risks are preserved in expectation across splits. It is also possible to perform risk estimation via various types of resampling methods, including both parametric and non-parametric forms of the bootstrap [8, 9]. Of particular relevance to this paper is the *wild bootstrap* (e.g., [29, 17, 16, 18]), a bootstrapping procedure that is well-suited to heteroskedastic data; we discuss it at more length below. For problems with particular structure, other more specialized methods are available. Notably, if one is willing to assume that the effective noise $Y - f^*(X)$ follows a Gaussian distribution, then Stein's unbiased estimate of risk [22], along with the associated family of covariance-based penalties [8], can be used for risk estimation. It is also possible to combine bootstraps with covariance-based penalties [24].

It should be noted that many methods—among them cross-validation and various types of covariance-based penalties—do *not* provide estimates of the risk $\bar{\mathcal{R}}(\hat{f})$; this risk is itself a random variable, due to the data used to train \hat{f} . Instead, such methods are targeting the deterministic quantity obtained by averaging $\bar{\mathcal{R}}(\hat{f})$ over the training data. Bates et al. [3] provide discussion of this distinction and related subtleties in the context of cross-validation. To make this distinction clear, we refer to the random variable $\hat{R}_n(\hat{f})$ —or the corresponding excess risk $\bar{\mathcal{E}}(\hat{f})$ —as the *instance-wise risk*.

1.2 Contributions

This paper is motivated by the goal of obtaining a method for risk estimation with the following properties:

- (a) For a given predictor \hat{f} , it provides an estimate of the instance-wise risk $\hat{R}_n(\hat{f})$ (or the instance-wise excess risk $\bar{\mathcal{E}}(\hat{f})$), and this estimate is equipped with an explicit and non-asymptotic guarantee.
- (b) It allows for heteroskedasticity, and other forms of heterogeneity in the distribution of pairs (x_i, y_i) used to fit the predictor \hat{f} .
- (c) It requires only black-box access to the statistical method \mathcal{M} for producing predictors—that is, we can re-fit the method for a new dataset, but we have no visibility into its inner structure.
- (d) It makes a limited number of queries to the method \mathcal{M} .

Let us provide some motivation for these desiderata. Beginning with requirement (a), it is desirable to target the instance-wise risk $\bar{\mathcal{R}}(\hat{f})$, since it correctly reflects the mean-squared error

¹There are relaxations of the i.i.d. condition, but the essential requirement is that the risks across different splits of the dataset are equivalent.

that will be achieved by applying the given predictor \hat{f} —with the underlying training data held fixed—on future data. Non-asymptotic bounds are desirable in that they are explicit and hold for all sample sizes (as opposed to an asymptotic statement). Re requirement (b), modern datasets often exhibit various forms of heterogeneity, so it is desirable to weaken independence or exchangeability assumptions as much as possible. As for the black-box requirement in item (c), many methods in modern statistics and machine learning are relatively complex, and it is desirable to have methods for risk estimation that do not require explicit knowledge about their structure. Deep neural networks, which are widely used for prediction, are a canonical instance of such an opaque model. Lastly, the limited query condition is item (d) is also important in modern statistical practice; the training process required to fit a method \mathcal{M} can be quite expensive, so it is undesirable to have a procedure (e.g., such as a typical bootstrap) that requires repeated re-fitting of the model a large number of times.

In this paper, we describe a procedure for risk estimation that is equipped with properties (a) through (d). It is inspired by a classic line of work on the wild bootstrap (e.g., [29, 17, 16, 19]), and for this reason, we refer to it as the *wild refitting procedure*. At its core is a form of Rademacher symmetrization applied to a set of estimated residuals; see [Section 2.3](#) for a detailed description. This type of Rademacher symmetrization is standard in the analysis of uniform laws of large numbers and related empirical processes [26, 25, 28]. In the context of the wild bootstrap, it has also been proposed and studied [17, 19, 18], with theoretical results given on its asymptotic behavior. In contrast, we analyze this form of Rademacher in a non-asymptotic setting, making essential use of the sharp concentration properties of Lipschitz functions of Rademacher variables [15].

Organization: The remainder of this paper is organized in follows. We begin in [Section 2.1](#) by setting up the problem, whereas [Section 2.2](#) is devoted to the notion of *optimism* that distinguishes between the population and empirical risks. In [Section 2.3](#), we describe the wild refitting procedure that is the main focus of this paper, and we provide a simple illustration of its behavior in [Section 2.4](#). Our main theoretical results are given in [Section 3](#), including [Theorem 1](#) that bounds the excess risk in terms of a quantity known as the wild optimism, and [Theorem 2](#) that shows how to bound the statistical estimation error. In [Section 4](#), we report the results of some numerical studies, where we illustrate the use of wild refitting for non-rigid structure-from-motion recovery ([Section 4.1](#)) and image denoising methods using plug-and-play methods with deep neural net priors ([Section 4.2](#)). We provide proofs in [Section 5](#), and conclude with a discussion in [Section 6](#).

2 Problem set-up

In this section, we begin by setting up the problem more precisely, before describing the wild refitting procedure that we study in this paper.

2.1 *M*-estimation and fixed design prediction

Given a covariate-response pair (X, Y) , the optimal function f^* for generating predictions $x \mapsto \hat{y}$ is given by the *regression function* $f^*(x) := \mathbb{E}[Y | X = x]$. Thus, given a collection of n covariate-response pairs (x_i, y_i) , they can be viewed as generated from the model

$$y_i = f^*(x_i) + w_i \quad \text{for } i = 1, \dots, n$$

where each w_i is a realization of a conditionally zero-mean random variable W_i (i.e., such that $\mathbb{E}[W_i | X_i = x_i] = 0$.) The focus of this paper is the *fixed design* case, where we condition upon the given realization $\{x_i\}_{i=1}^n$ of the covariates, and compute prediction errors using the empirical distribution \mathbb{P}_n that places mass $1/n$ at each x_i .

On one hand, this type of conditional analysis can be performed for any prediction problem; moreover, there are many prediction problems where it is most natural to view the covariates as fixed. Examples include prediction of a time series, where covariates correspond to particular points in time; and prediction in images or video, where covariates correspond to particular two-dimensional spatial positions (for an image), or 2D-space-time positions (for a video).

Prediction via M -estimation: In this paper, we study prediction methods that are specified by a real-valued class \mathcal{F} of functions on the covariate space \mathcal{X} , and a penalty function $\mathcal{P} : \mathcal{F} \rightarrow \mathbb{R}$. Given a data set $\{(x_i, y_i)\}_{i=1}^n$, we obtain the fitted predictor \hat{f} by solving the optimization problem

$$\hat{f} \in \arg \min_{f \in \mathcal{F}} \left\{ \frac{1}{n} \sum_{i=1}^n (y_i - f(x_i))^2 + \mathcal{P}(f) \right\}. \quad (2)$$

In general, procedures of this type are referred to as non-parametric M -estimators; in this paper, we are analyzing the case of non-parametric and penalized least-squares.

Let us summarize some shorthand notation that we use throughout the remainder of this paper. For a pair of real-valued functions f and g defined on the covariate space \mathcal{X} , we define the squared norm

$$\|f - g\|_n^2 := \frac{1}{n} \sum_{i=1}^n (f(x_i) - g(x_i))^2 \quad (3a)$$

along with the associated inner product

$$\langle f, g \rangle_n := \frac{1}{n} \sum_{i=1}^n f(x_i)g(x_i). \quad (3b)$$

2.2 Excess risk and optimism

Given a predictor \hat{f} , recall the definition (1) of its population excess risk. Given the fixed design set-up of this paper, this population excess risk takes the form

$$\bar{\mathcal{E}}(\hat{f}) = \underbrace{\frac{1}{n} \sum_{i=1}^n (\hat{f}(x_i) - f^*(x_i))^2}_{\equiv \|\hat{f} - f^*\|_n^2}, \quad (4a)$$

corresponding to the *mean-squared error* or MSE between \hat{f} and f^* evaluated on the fixed covariates $\{x_i\}_{i=1}^n$.

In analogy to the population excess risk (1), given a data set $\{(x_i, y_i)\}_{i=1}^n$, we can also define the *empirical excess risk* as

$$\hat{\mathcal{E}}_n(\hat{f}) := \frac{1}{n} \sum_{i=1}^n (y_i - \hat{f}(x_i))^2 - \frac{1}{n} \sum_{i=1}^n (y_i - f^*(x_i))^2. \quad (4b)$$

In contrast to the population case, the empirical excess risk need not be non-negative.

The difference between the population and empirical excess risks defines the *optimism* of an estimate \hat{f} . For the least-squares objective considered here, some simple algebra yields

$$\bar{\mathcal{E}}(\hat{f}) = \hat{\mathcal{E}}_n(\hat{f}) + 2 \text{Opt}^*(\hat{f}) \quad \text{where} \quad \text{Opt}^*(\hat{f}) := \underbrace{\frac{1}{n} \sum_{i=1}^n w_i (\hat{f}(x_i) - f^*(x_i))}_{\equiv \langle w, \hat{f} - f^* \rangle_n}, \quad (5)$$

where $w_i := y_i - f^*(x_i)$ is the effective noise in the regression model. Thus, in order to obtain an upper bound on the population excess risk, it suffices to obtain an upper bound on the optimism $\text{Opt}^*(\hat{f})$.

2.3 Wild refitting

The main contribution of this paper is to demonstrate the effectiveness—both empirically and theoretically—of a simple refitting procedure for computing upper bounds on the optimism, and hence the population excess risk. As noted earlier, we refer to this method as *wild refitting*, since like one variant of the wild bootstrap (e.g., [29, 17, 16, 19]), it makes use of random signs (Rademacher variables) to symmetrize an appropriate set of residuals, and also allows for general heteroskedasticity. Note that $\text{Opt}^*(\hat{f})$ is a random variable, since it depends on both the noise terms w_i and estimate \hat{f} itself. Thus, the wild refitting procedure also returns a random variable.

While our theoretical analysis focuses on M -estimators of the form (2), the procedure itself applies to any statistical method \mathcal{M} that uses an n -vector y of responses to compute a predictor $\tilde{f} := \mathcal{M}(y)$ belonging to some function space \mathcal{F} . Any instantiation of the wild refitting procedure depends on a recentering predictor $\tilde{f} : \mathcal{X} \rightarrow \mathbb{R}$ and a scalar noise level $\rho > 0$. It requires only black-box access to the estimator \mathcal{M} , that we can compute the function $\mathcal{M}(u) \in \mathcal{F}$ for any possible response vector $u \in \mathbb{R}^n$.

Wild Refitting

Inputs: Prediction method $\mathcal{M} : \mathbb{R}^n \rightarrow \mathcal{F}$

Response vector $y \in \mathbb{R}^n$ and fitted predictor $\hat{f} = \mathcal{M}(y)$

Recentering predictor $\tilde{f} \in \mathcal{F}$ and noise scale $\rho > 0$.

- (i) With the given recentering function \tilde{f} , compute the residuals

$$\tilde{w}_i := y_i - \tilde{f}(x_i) \quad \text{for } i = 1, 2, \dots, n. \quad (6a)$$

- (ii) Using original predictor \hat{f} and given noise scale $\rho > 0$, form the wild responses

$$y_i^\bullet := \hat{f}(x_i) + \underbrace{\rho \varepsilon_i \tilde{w}_i}_{=: w_i^\bullet} \quad \text{for } i = 1, \dots, n, \quad (6b)$$

where $\{\varepsilon_i\}_{i=1}^n$ is an i.i.d. sequence of Rademacher variables.

- (iii) Compute the refitted wild solution $f_\rho^\bullet := \mathcal{M}(y^\bullet)$.

Outputs:

- Wild refit f_ρ^\bullet
- Wild noise vector $w_\rho^\bullet = (w_i^\bullet)_{i=1}^n$

} \implies Use to bound excess risk
 $\bar{\mathcal{E}}(\hat{f})$ via suitable choice of ρ

In the simplest instantiation, we use the estimate \hat{f} itself as the centering function (i.e., $\tilde{f} \equiv \hat{f}$), but as our theory clarifies, other choices of the centering function \tilde{f} can yield superior performance. Moreover, the noise scale ρ plays an important role, and our theory provides guidance on its choice.

The wild-refitting problem can be used to define an optimism term, given by

$$\widetilde{\text{Opt}}^\bullet(f_\rho^\bullet) := \frac{1}{n} \sum_{i=1}^n \varepsilon_i \tilde{w}_i (f_\rho^\bullet(x_i) - \hat{f}(x_i)). \quad (7)$$

In contrast to the true optimism $\text{Opt}^*(\hat{f})$, this wild optimism depends only on quantities that can be computed based on the original observation vector $y \in \mathbb{R}^n$, along with the Rademacher sequence $\varepsilon \in \{-1, +1\}^n$ introduced as part of the wild-refitting procedure. The main results of this paper are to establish conditions under which the quantities defining this wild optimism can be used to bound the true optimism, and hence the true excess risk.

Notably—and in sharp contrast to asymptotic or distributional guarantees provided by the wild bootstrap—we will provide guarantees that hold based on a *single realization* of the Rademacher vector $\varepsilon \in \{-1, +1\}^n$. Thus, we do not provide distributional guarantees, but instead a non-asymptotic guarantee. Moreover, the wild refitting procedure only requires a single call to the prediction method \mathcal{M} , as laid out in item (d) of our motivating desiderata (see [Section 1.2](#)).

2.4 A simple illustration: Tikhonov versus TV regularization

So as to provide intuition, let us begin by considering a simple form of model selection in the context of non-parametric regression. Let $f^* : [0, 1] \rightarrow \mathbb{R}$ be the unknown regression function, and

suppose that we collect n noisy observations of the form

$$y_i = f^*(x_i) + w_i \quad \text{where } x_i = i/n \text{ for } i = 1, \dots, n, \quad (8)$$

and $\{w_i\}_{i=1}^n$ is an i.i.d. sequence of zero-mean noise variables. Various classical approaches are based on M -estimators of the form (2) with suitable penalty functions. Here we consider two methods based on penalties from the family

$$\mathcal{P}_q(f) = \sum_{i=1}^{n-1} |f(x_{i+1}) - f(x_i)|^q \quad \text{for an exponent } q \geq 0.$$

The choice $q = 2$ corresponds to *Tikhonov regularization*, whereas the choice $q = 1$ corresponds to a *total variation* (TV) method.

The TV estimator imposes a sparsity constraint on the function differences, and so is well-suited to reconstructing functions with step-like behavior. On the other hand, Tikhonov regularization imposes a type of smoothness penalty, and so is better suited to smoother functions. So as to illustrate these trade-offs, we constructed a family of functions that vary from step-like to smooth. We began by constructing a function $f_0^* : [0, 1] \rightarrow \mathbb{R}$ that is piecewise constant, with three distinct pieces, as illustrated in the left-most panel in the top row of Figure 1. By convolving this function with a zero-mean Gaussian with variance γ^2 , we obtain a sequence of progressively smoother functions f_γ^* , as shown in the top row panels moving left to right. Thus, the left-most function is best suited to TV regularization, whereas the right-most function is best suited to Tikhonov regularization.

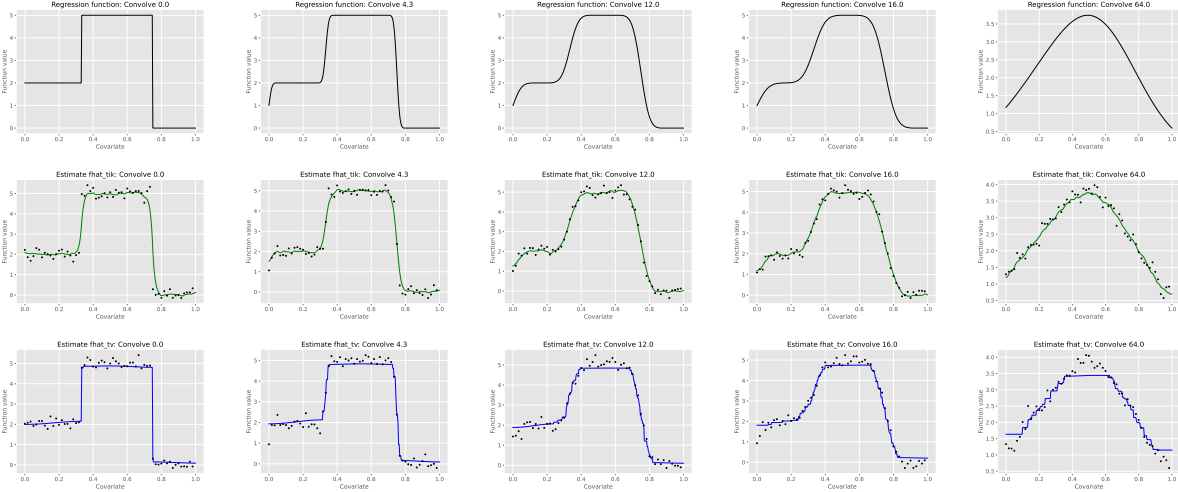


Figure 1. Top row: illustration of the family of functions f_γ^* for different choices of the smoothing parameter $\gamma \geq 0$. Middle row: Corresponding function estimate \hat{f} with Tikhonov regularization. Bottom row: corresponding function estimates with TV regularization.

We then applied both the Tikhonov and the TV estimates to observations from the model (8) for the γ -convolved function f_γ^* over a range of convolution strengths γ . Panel (a) of Figure 2 plots the excess risk $\bar{\mathcal{E}}(\hat{f})$ of the Tikhonov estimate versus γ , and compares it to the wild estimates

of excess risk for wild noise scales $\rho \in \{1.0, 1.2, 1.4\}$. Panel (b) provides these same plots for the TV estimate. Consistent with the smoothness/sparsity interpretation, note that the MSE of the Tikhonov method decreases as γ increases, whereas that of the TV method exhibits the opposite behavior. Note also how the wild-estimated MSEs track this behavior.

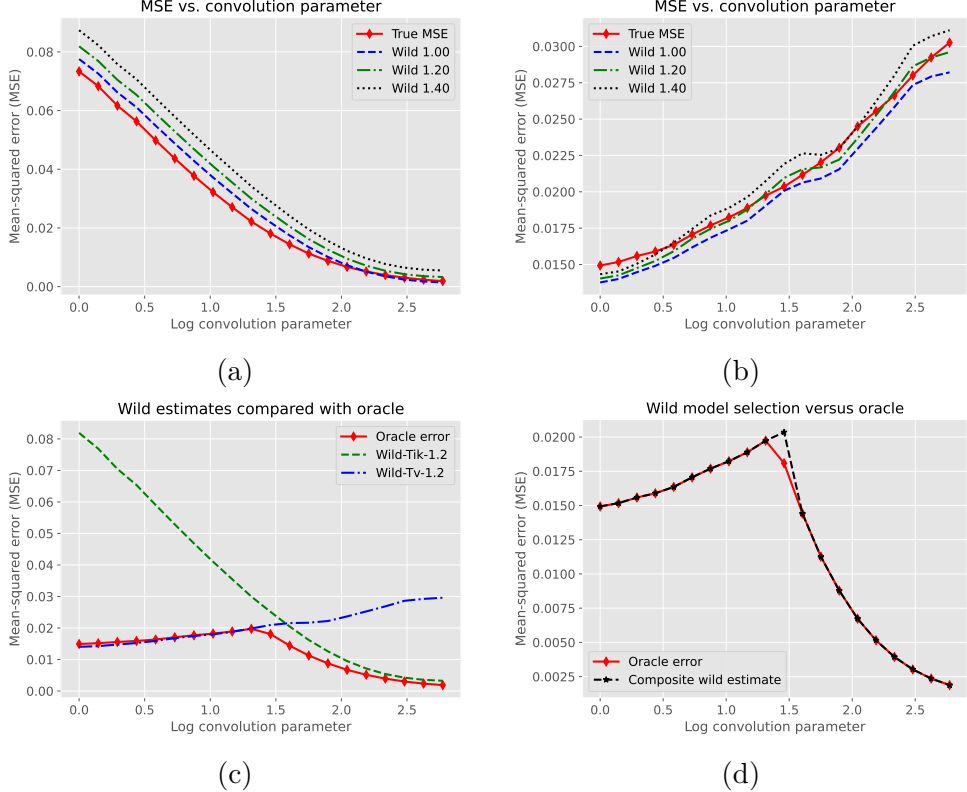


Figure 2. Panels (a) and (b): Comparison of the true MSE $\bar{\mathcal{E}}(\hat{f})$ and wild estimates at noise scales $\rho \in \{1.0, 1.2, 1.4\}$ for the Tikhonov estimate (panel (a)) and the TV estimate (panel (b)). (c) Plots of the MSE obtained by an oracle (red diamonds) that can choose optimally between the two estimators. (d) Comparison of model selection using the wild estimates to the oracle error.

In panel (c) of Figure 2, we plot (in red diamonds) the MSE obtained by the *oracle selector* that chooses, for each value of γ , between the TV and Tikhonov estimate so as to minimize the MSE. We refer to the MSE obtained in this as the oracle MSE. We also overlay the wild estimates of the MSEs of these two methods. In panel (d), we plot the oracle MSE (red diamonds) versus the MSE obtained by wild model selection (black stars). The latter method performs model selection based on the wild-estimated MSEs shown in panel (c).

3 Analysis and non-asymptotic guarantees

We now turn to some analysis of the wild refitting procedure, in particular in the form of non-asymptotic guarantees on the wild optimism. In this section, we prove two main results:

- Theorem 1 gives an upper bound on the true optimism in terms of the wild optimism $\widetilde{\text{Opt}}^*(f_\rho^*)$

evaluated at an appropriate wild noise scale ρ . However, this choice depends on the estimation error $\hat{r}_n := \|\hat{f} - f^\dagger\|_n$, which is unknown.

- [Theorem 2](#) closes this gap by showing how wild refitting can be used to generate a high-probability upper bound on \hat{r}_n . This bound provides guidance on the setting of wild noise scale for which the guarantee from [Theorem 1](#) holds.

3.1 Problem set-up and wild complexity

Our analysis applies to an estimate \hat{f} generated by solving an optimization problem of the form (2). Given this structure, it is natural to define

$$f^\dagger = \arg \min_{f \in \mathcal{F}} \left\{ \|f - f^*\|_n^2 + \mathcal{P}(f) \right\}, \quad (9)$$

corresponding to the best penalized approximation to f^* in the absence of any noise. Note that f^\dagger is a deterministic function, since we are viewing the covariates as fixed.

3.1.1 Assumptions

We now describe the assumptions that underlie our analysis.

Firm non-expansiveness: For a given function $f \in \mathcal{F}$, introduce the convenient shorthand $f(x_1^n) := (f(x_1), \dots, f(x_n)) \in \mathbb{R}^n$. In the bulk of our analysis, we focus on penalty functions $\mathcal{P} : \mathcal{F} \rightarrow \mathbb{R}^+$ of the form

$$\mathcal{P}(f) := \begin{cases} 0 & \text{if } f(x_1^n) \in \mathcal{C}, \text{ and} \\ +\infty & \text{otherwise,} \end{cases} \quad (10)$$

where $\mathcal{C} \subset \mathbb{R}^n$ is a given compact subset of \mathbb{R}^n . In future work, we will explore theoretical extensions to regularized estimators in the Lagrangian case.

Our analysis requires that the resulting method $\mathcal{M} : \mathbb{R}^n \rightarrow \mathcal{F}$, as defined in by equation (2), be *firmly non-expansive* around f^* . More precisely, noting that $f^\dagger = \mathcal{M}(f^*(x_1^n))$ by assumption, we require that the estimate $\tilde{f} = \mathcal{M}(f^*(x_1^n) + u)$ obtained from via any perturbation vector $u \in \mathbb{R}^n$ satisfies the inequality

$$\underbrace{\|\mathcal{M}(f^*(x_1^n) + u) - \mathcal{M}(f^*(x_1^n))\|_n^2}_{\equiv \|\tilde{f} - f^\dagger\|_n^2} \leq \langle u, \tilde{f} - f^\dagger \rangle_n. \quad (11a)$$

When the set \mathcal{C} is convex, then this firm-expansiveness follows from standard optimization-theoretic properties of projections onto convex sets (e.g., [12]). It is worth noting, however, that a local property of this type can hold more generally for certain non-convex sets (e.g., prox-regular sets [21]).

Noise conditions: Recall that our observations take the form $y_i = f^*(x_i) + w_i$, where each w_i is an additive noise variable. We require that

$$\text{Conditioned on } \{x_i\}_{i=1}^n: \quad (w_1, \dots, w_n) \text{ are independent, each with symmetric distribution.} \quad (11b)$$

The conditional symmetry assumption implies that $\mathbb{E}[w_i \mid x_i] = 0$, a fact that we exploit in our analysis. When the symmetry condition fails to hold, the bounds that we give here all hold with an increased constant factor. (Essentially, we lose a factor of two in order to handle non-symmetric noise, since we need to introduce two separate copies of w and w' , and take their difference in order to form the symmetrized analog.)

Remark: Other than the conditions (11b), we impose no other assumptions on the noise variables. In particular, they are permitted to be heteroskedastic and/or exhibit highly non-Gaussian tail behavior.

3.1.2 From wild optimism to wild complexity

For future reference, it is convenient to highlight an important connection between the wild optimism, and a function $r \mapsto W_n(r)$ that we refer to as the wild complexity. Recall that the *wild optimism* at noise scale ρ for the estimate \hat{f} is given by

$$\widetilde{\text{Opt}}^*(f_\rho^*) := \frac{1}{n} \sum_{i=1}^n \varepsilon_i \tilde{w}_i (f_\rho^*(x_i) - \hat{f}(x_i)), \quad \text{where } \tilde{w}_i = y_i - \tilde{f}(x_i). \quad (12a)$$

Here \tilde{f} is the pilot estimator (frequently equal to \hat{f}), and $f_\rho^* = \mathcal{M}(y^*)$ is the method applied to the wild observations $y_i^* = \hat{f}(x_i) + \rho \varepsilon_i \tilde{w}_i$. On the other hand, the *wild noise complexity* at \hat{f} is the function given by

$$r \mapsto W_n(r) := \sup_{f \in \mathbb{B}_r(\hat{f})} \left[\frac{1}{n} \sum_{i=1}^n \varepsilon_i \tilde{w}_i (f(x_i) - \hat{f}(x_i)) \right]. \quad (12b)$$

This wild noise complexity is intimately related to the wild optimism, as formalized by the following result:

Lemma 1 (From wild optimism to wild complexity). *For any wild noise scale $\rho > 0$, we have*

$$\widetilde{\text{Opt}}^*(f_\rho^*) = W_n(\|f_\rho^* - \hat{f}\|_n). \quad (13)$$

See [Section 7](#) for the proof of this claim.

3.2 Bounding the true optimism

With these ingredients in place, we are now ready to state a high-probability bound on the true optimism $\text{Opt}^*(\hat{f})$ in terms of the wild optimism $\widetilde{\text{Opt}}^*(f_\rho^*)$.

Theorem 1 (Wild optimism bound). *Under the noise condition (11b), consider any radius r such that $\|\widehat{f} - f^\dagger\|_n \leq r$, and let $\rho > 0$ be the noise scale for which $\|f_\rho^* - \widehat{f}\|_n = 2r$. Then for any $t > 0$, we have*

$$\text{Opt}^*(\widehat{f}) \leq \widetilde{\text{Opt}}^*(f_\rho^*) + \{H_n(t) + A_n(\widetilde{f})\} \quad \text{with prob. at least } 1 - 4e^{-t^2}, \quad (14)$$

where the probability deviation term is given by

$$H_n(t) := \{3r + \|f^\dagger - f^*\|_n\} \frac{2\|w\|_\infty t}{\sqrt{n}} \quad (15a)$$

and the pilot error is given by

$$A_n(\widetilde{f}) := \sup_{f \in \mathbb{B}_{2r}(\widehat{f})} \frac{1}{n} \sum_{i=1}^n \varepsilon_i (\widetilde{f}(x_i) - f^*(x_i)) (f(x_i) - \widehat{f}(x_i)). \quad (15b)$$

See [Section 5.1](#) for the proof of this theorem.

To interpret this result, note that inequality (14) shows that the true optimism $\text{Opt}^*(\widehat{f})$ can be upper bounded by the wild optimism for an *appropriately chosen* ρ , along with the probability deviation term (15a) and the pilot error term (15b). Let us comment on these two terms.

Probability deviation term: The guarantee holds with exponentially high probability (i.e., $1 - 4e^{-t^2}$) in the deviation term t ; this sharp tail behavior arises due to the highly favorable concentration behavior of Rademacher variables used the wild refitting procedure. Our proof exploits concentration inequalities for convex and Lipschitz functions of Rademacher variables so as to preserve this behavior. The function $H_n(t)$ defined in equation (15a) scales as $t\|w\|_\infty/\sqrt{n}$, so that the distributional properties of the additive noise vector $w \in \mathbb{R}^n$ enter purely via the sup-norm $\|w\|_\infty$. This fact means that it is possible to handle noise with tail behavior much heavier than Gaussian. For example, consider a noise distribution that has only a finite polynomial moment—say $\mathbb{E}|w|^k \leq C$ for some $k > 2$. An easy calculation shows that $\mathbb{E}\|w\|_\infty \leq (Cn)^{1/k}$, with similar bounds for the event $\{\|w\|_\infty \geq s\}$, so that [Theorem 1](#) can still yield non-trivial guarantees. We illustrate the behavior of the wild-refitting procedure for heavy-tailed Student t -noise in [Section 4.2](#); in particular, see [Figure 7](#).

Pilot error term: Now let us consider the pilot error term (15b), and in particular its relation to the wild optimism. From the equivalence (13), the wild optimism in the bound (14) can be written as

$$\widetilde{\text{Opt}}^*(f_\rho^*) = W_n(2r) = \sup_{f \in \mathbb{B}_{2r}(\widehat{f})} \frac{1}{n} \sum_{i=1}^n \varepsilon_i \tilde{w}_i (f(x_i) - \widehat{f}(x_i)).$$

By comparison with the definition (15b), we see that the pilot error has the same form, with the residual \tilde{w}_i replaced by the difference $d(x_i) := \widetilde{f}(x_i) - f^*(x_i)$. Consequently, as long as the pilot function \widetilde{f} is a reasonable estimate f^* —so that the difference $d(x_i)$ is typically smaller than the noise w_i —then we can expect that the pilot error is dominated by $\widetilde{\text{Opt}}^*(f_\rho^*)$.

3.3 Bounding the estimation error

The key assumption in [Theorem 1](#) is the existence of some known r such that $r \geq \|\hat{f} - f^*\|_n$. Thus, it becomes useful only in so far as we can obtain an upper bound on the *statistical estimation error* $\hat{r}_n := \|\hat{f} - f^\dagger\|_n$. This quantity corresponds to the error associated with estimating the best approximation f^\dagger to f^* from the chosen function class \mathcal{F} (cf. equation [\(9\)](#)). In this section, we describe an explicit procedure that can be used to obtain upper bounds on \hat{r}_n . It involves an inequality defined in the terms of the wild complexity $W_n(r)$ from equation [\(12b\)](#).

Theorem 2 (Estimation error bounds via wild complexity). *Under the non-expansive condition [\(11a\)](#) and the noise condition [\(11b\)](#), for any $t \geq 3$, we have*

$$\hat{r}_n^2 \leq \max \left\{ W_n((2 + \frac{1}{t})\hat{r}_n), \frac{t^4}{n} \right\} + \frac{6\|w\|_\infty}{t} \hat{r}_n^2 + A_n(\tilde{f}) \quad (16a)$$

with probability at least $1 - 2e^{-t^2}$. Moreover, if \mathcal{F} is convex, then with the same probability, for any noise scale $\rho > 0$, we have

$$\hat{r}_n^2 \leq \max \left\{ (r_\rho^\bullet)^2, \frac{\hat{r}_n}{r_\rho^\bullet} W_n((2 + \frac{1}{t}) r_\rho^\bullet), \frac{t^4}{n} \right\} + \frac{6\|w\|_\infty}{t} \hat{r}_n^2 + A_n(\tilde{f}), \quad (16b)$$

where $r_\rho^\bullet = \|f_\rho^\bullet - \hat{f}\|_n$ is the error of the wild refit f_ρ^\bullet .

See [Section 5.3](#) for the proof of this claim.

Let us make a few comments to interpret the meaning of the two bounds in the theorem. Both bounds involve the pilot error term $A_n(\tilde{f})$, as previously discussed, along with probability deviation parameter t and sup-norm $\|w\|_\infty$ of the noise vector. Focusing on the bound [\(16a\)](#), the t^4/n term within the maximum on the right-hand side is of lower order whenever $\hat{r}_n^2 \gtrsim 1/n$, which is the case in all but the simplest parametric problem. Disregarding these terms, the rough interpretation is that we have an upper bound of the form $\hat{r}_n \leq r$ for any radius r such that

$$r^2 \geq W_n((2 + \frac{1}{t})r). \quad (17)$$

Finding the best such bound amounts to finding the smallest radius r that satisfies this inequality. Note that this can be done, because for a given radius s , the wild complexity $W_n(s)$ is computable based purely on the given estimate \hat{f} , along with the wild noise variables $\{\tilde{w}_i\}_{i=1}^n$. Alternatively, from the equivalence [\(13\)](#) from [Lemma 1](#), we can compute $W_n(s)$ by varying the wild noise scale ρ until the wild estimate f_ρ^\bullet satisfies $\|f_\rho^\bullet - \hat{f}\|_n = s$. On the other hand, the bound [\(16b\)](#) is a slightly weaker but more interpretable result that holds for convex function classes. We discuss its use and geometric meaning below.

3.4 Putting together the pieces

Let us now summarize the overall conclusions that can be drawn from [Theorems 1](#) and [2](#) in conjunction, focusing on the case of a convex function class \mathcal{F} . Consider the problem of upper bounding $\hat{r}_n = \|\hat{f} - f^\dagger\|_n$. If we disregard the deviation and approximation terms, then a rough summary of

the bound (16b) is via the inequality

$$\hat{r}_n \leq \max \left\{ r_\rho^*, \frac{W_n(2r_\rho^*)}{r_\rho^*} \right\} \stackrel{(\dagger)}{\leq} \underbrace{\max \left\{ r_\rho^*, \frac{2W_n(r_\rho^*)}{r_\rho^*} \right\}}_{\equiv B(\rho)} \quad (18)$$

Here inequality (\dagger) follows from the concavity of the function $u \mapsto W_n(u)$, which implies that $u \mapsto W_n(u)/u$ is decreasing. See [Lemma 7](#) in [Section 5.3.2](#) for details.

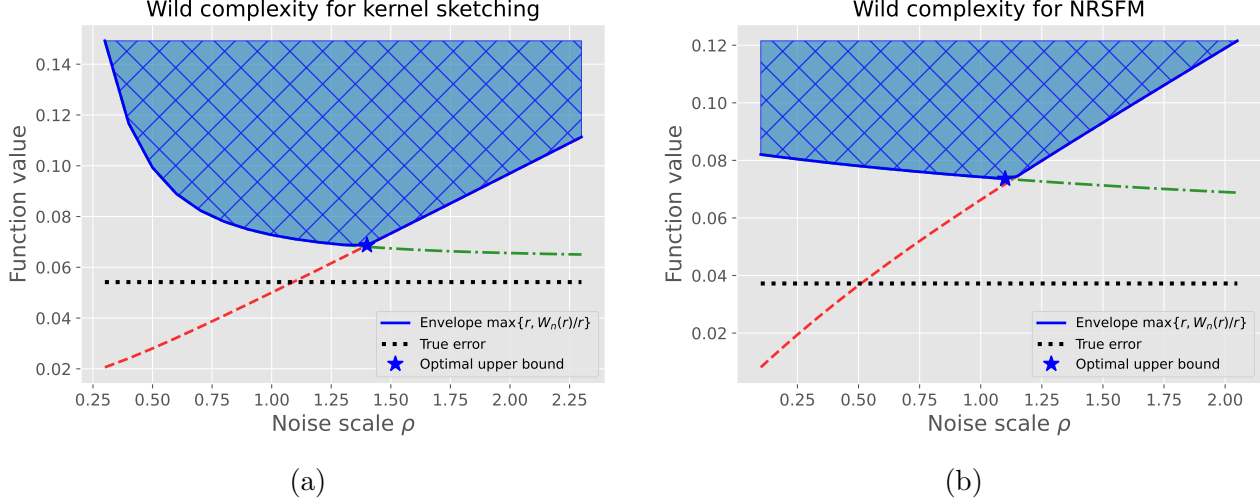


Figure 3. The family of inequalities defined by the functions (19) can be used to compute upper bounds on the true error $\hat{r}_n = \|\hat{f} - f^\dagger\|_n$. Illustrated for two different prediction problems: (a) Randomized sketching approximations for kernel ridge regression [30]. (b) Non-rigid structure-from-motion ([Section 4.1](#)).

Observe that the bound (18) holds for each choice of noise scale ρ ; consequently, we can optimize this choice so as to obtain the tightest possible bound. The function $\rho \mapsto B(\rho)$ defined in equation (18) is the maximum of the two functions

$$B_1(\rho) := r_\rho^*, \quad \text{and} \quad B_2(\rho) := \frac{2W_n(r_\rho^*)}{r_\rho^*} \quad \text{where } r_\rho^* := \|f_\rho^* - \hat{f}\|_n. \quad (19)$$

In [Figure 3](#), we plot these two functions versus ρ for two different problems: (a) randomized sketching approximations for kernel ridge regression [30]; and (b) non-rigid structure-from-motion (see [Section 4.1](#) for details on the latter application).

The error r_ρ^* is an increasing function² of the noise scale ρ , so that the function B_1 is increasing in ρ . In [Figure 3](#), this increasing function is plotted with a red-dotted line. On the other hand, as noted above, the function $u \mapsto W_n(u)/u$ is decreasing u , which implies that the function B_2 is decreasing in the wild noise scale ρ . This decreasing function is shown with a dashed-dotted green line in [Figure 3](#). The maximum of the two functions (i.e., $\rho \mapsto \max\{B_1(\rho), B_2(\rho)\}$), plotted in a solid blue line, provides an upper bound on $\hat{r}_n = \|\hat{f} - f^\dagger\|_n$. We can find the optimal bound by varying the noise scale ρ up to the point where $B_1(r_\rho^*) = B_2(r_\rho^*)$, or equivalently $r_\rho^* = 2 \frac{W_n(r_\rho^*)}{r_\rho^*}$. This optimal upper bound is marked in the plots with a blue star.

²Our use of increasing does not mean strictly so; we are using increasing in the sense of non-decreasing.

Once we have obtained an upper bound on \hat{r}_n , we can then return to [Theorem 1](#). It suggests that—apart from the higher-order and pilot terms—we can upper bound the true optimism $\text{Opt}^*(\hat{f})$ via the wild optimism $\widetilde{\text{Opt}}^*(f_\rho^*)$ for the noise scale that we have chosen. Finally, we combine this upper bound on the optimism with equation (5) so as to upper bound the excess risk.

4 Some numerical studies

In this section, we illustrate the performance of wild refitting on two different classes of problems:

- [Section 4.1](#): we predict the excess risk for low-rank matrix estimators used for recovery in non-rigid shape-from-motion. We illustrate how the wild refitting method can be used to select an appropriate rank for a standard method based on low-rank matrix approximation [7].
- [Section 4.2](#): we illustrate its behavior for plug-and-play denoising methods based on deep neural network priors.

4.1 Non-rigid structure-from-motion

We begin by illustrating the wild refitting procedure in application to the problem of non-rigid structure-from-motion (NRSFM) recovery, which is a standard problem in computer vision with a lengthy history (e.g., [4, 1, 7]). In our illustration, we focus on a NRSFM recovery method based on low-rank matrix approximation, as described by Dai et al. [7].

For a given instance of NRSFM recovery, the dataset consists of m observations of a collection of p points. Each frame is taken by a camera at a particular time and position, and each point represents a marker associated with some type of non-rigid moving object. In the CMU MoCap dataset [5] used for this investigation, each point corresponds to a marker on the moving object. The points lie in $3d$ space, but this $3d$ -location is unknown to us; instead, each frame of the camera sequence gives a $2d$ -projection of the unknown $3d$ -position for each point. By suitable algebraic re-arrangement, the full dataset can be described by a matrix $\mathbf{Y} \in \mathbb{R}^{2m \times p}$, where each point $j = 1, \dots, p$ is associated with a pair of rows in \mathbf{Y} .

Our goal is to recover the unknown *shape matrix* $\mathbf{S}^* \in \mathbb{R}^{3m \times p}$ that gives the $3d$ -positions of each of the p -points at each of the m frames. This unknown shape matrix is related to the observation matrix $\mathbf{Y} \in \mathbb{R}^{2m \times p}$ via the linear relationship

$$\mathbf{Y} = \mathbf{R}\mathbf{S}^* + \mathbf{W}, \quad (20a)$$

where $\mathbf{R} \in \mathbb{R}^{2m \times 3m}$ is a known camera-matrix for the $3d$ to $2d$ transformation in each frame, and $\mathbf{W} \in \mathbb{R}^{2m \times p}$ is an additive noise term.

Note that the observation matrix \mathbf{Y} contains a total of $2mp$ entries, whereas the unknown shape matrix \mathbf{S}^* has $3mp$ entries in total. Consequently, the problem is ill-specified without further restrictions, and it is essential to impose some form of regularity condition on \mathbf{S}^* . One widely-used approach is to assume that the shape matrix \mathbf{S}^* is relatively low-rank; this modeling assumption can be interpreted as the shape matrix being representable as a sum of a relatively small number of base shapes.

Given such a low-rank assumption, a natural convex estimator—as studied in the paper [7]—is to minimize a data-fidelity term subject to a constraint on the nuclear norm $\|\mathbf{S}\|_{\text{nuc}}$ of the shape

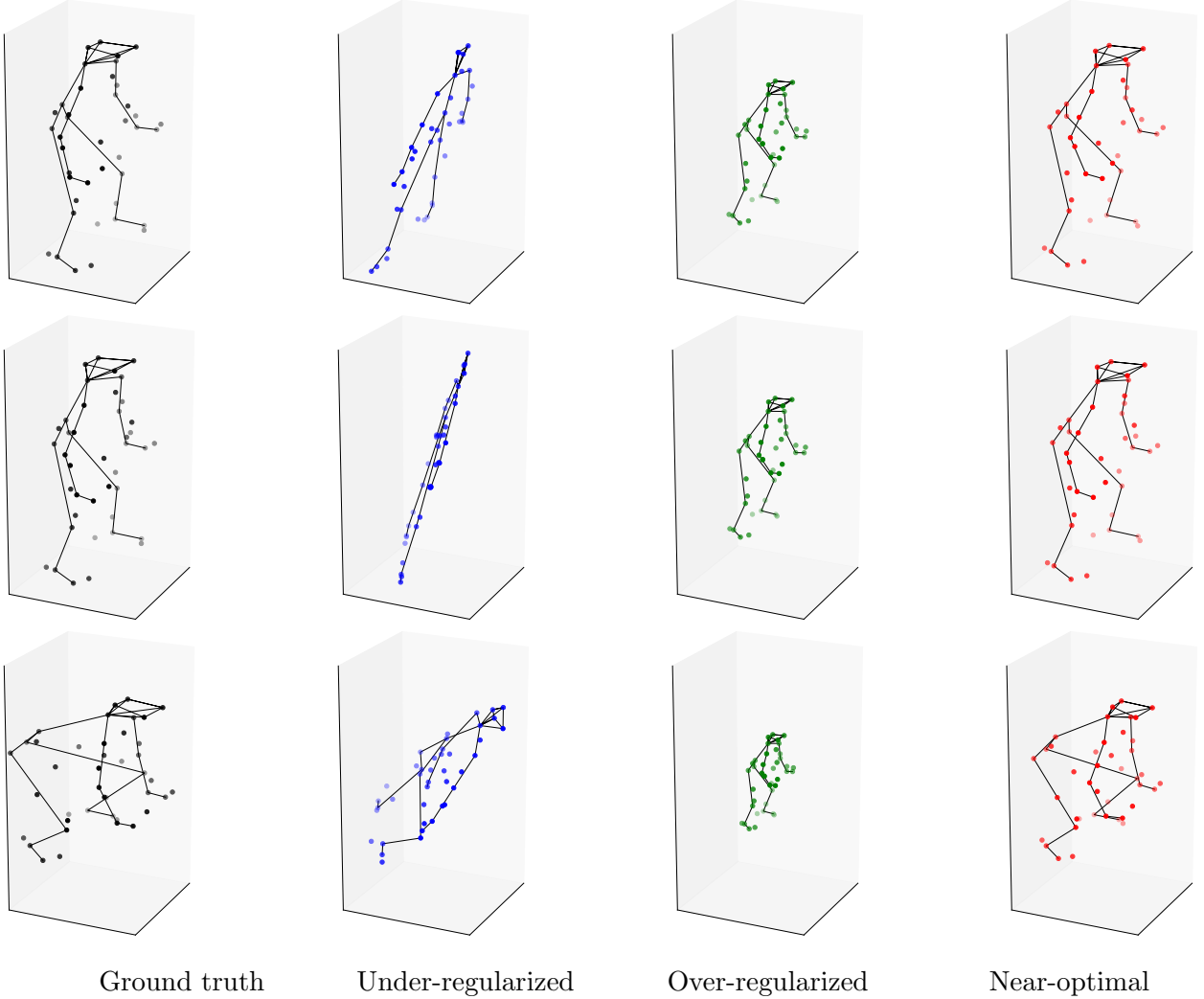


Figure 4. Comparison of reconstructed frames to ground truth for motion capture data (“Pick-up” sequence from the CMU motion capture dataset [5]). Reconstructions obtained by minimizing Frobenius norm subject to a nuclear norm constraint (20b) with three different choices of the radius r . First column: Three frames of ground truth movement, showing the part of the “Pick-up” movement. Second column: Under-regularized reconstruction (rank $r = 900$ is too large). Third column: Over-regularized reconstruction (rank $r = 200$ is too small). Fourth column: Reconstruction with rank $r = \exp(5.8) \approx 330$ chosen by the wild refitting procedure; see Figure 5 and surrounding discussion for details.

matrix. (The nuclear norm of a matrix can be viewed as a convex surrogate to the rank function, which is non-convex.) This combination leads to the family of estimators

$$\hat{\mathbf{S}}_r \in \arg \min_{\mathbf{S} \in \mathbb{R}^{3m \times p}} \|\mathbf{Y} - \mathbf{RS}\|_{\text{F}}^2 \quad \text{such that } \|\mathbf{S}\|_{\text{nuc}} \leq r, \quad (20b)$$

where $\|\cdot\|_{\text{F}}$ denotes the Frobenius norm, and $r \geq 0$ is the nuclear norm radius that we are free to choose. In practice, a “good choice” of r is essential in obtaining accurate reconstructions, and we

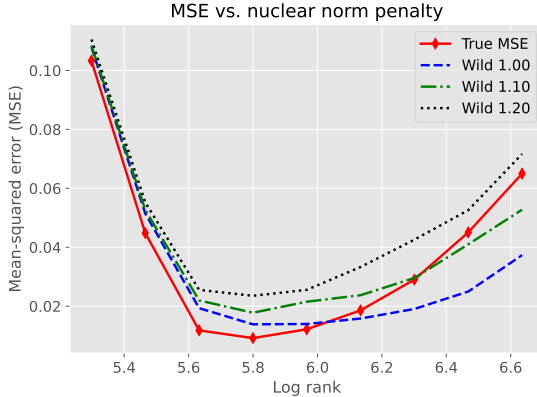


Figure 5. Plots of the true MSE (red solid line with diamonds) versus the log radius ($\log r$), and comparison with wild refitting estimates of the MSE for three different choices of the noise scale $\rho \in \{1.0, 1.1, 1.2\}$. Consistent with our theory, a sufficiently large value of ρ leads to an upper bound on the MSE. We used the wild-estimated MSE with $\rho = 1.2$ to select the radius; doing so leads to the choice $r^* = \exp(5.8) \approx 330$.

made use of the wild refitting procedure in order to make this choice, as we now describe.

Figure 4 shows results obtained by applying the nuclear norm constrained estimator (20b) to the ‘‘Pick-Up’’ sequence from the CMU MoCap database [5]. It consists of $p = 41$ points that are measured over a total of $m = 238$ frames. The left column in Figure 4 plots three of these frames for the ground truth dataset, which shows the basic form of the pick-up movement. (For clarity of the visualization, the plot also includes additional lines marking the body, but these are not part of the dataset itself.)

We then formed the data matrix \mathbf{Y} as in equation (20a), where the noise matrix \mathbf{W} had i.i.d. Gaussian entries with standard deviation $\sigma = 0.25$. We then solved the convex program (20b) for a wide range of nuclear norm radii r . The second, third and fourth panels in Figure 4 plot three frames of these reconstructions. The second column uses radius $r = 900$, leading to an under-regularized solution (stick figure spins around wildly), whereas the third column uses radius $r = 200$, leading to an over-regularized solution (stick figure simply shrinks). The final column shows three frames of the reconstruction using the radius $r^* \approx 330$, which is the choice suggested by our wild refitting procedure, which we describe next.

In order to choose the radius, we used the following version of wild refitting. Fixing collection of nine radii $r \in [200, 900]$, we performed the following steps for each r

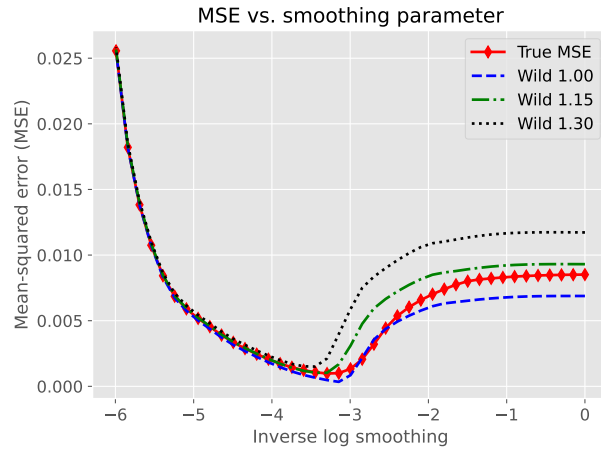
- we first computed the estimate $\widehat{\mathbf{S}}_r$ in equation (20b);
- then using this estimate, we computed the associated wild optimism $\widetilde{\text{Opt}}^\bullet(f_\rho^\bullet)$ for three different choices of wild noise scale—namely, $\rho \in \{1.0, 1.1, 2.2\}$.

We then used these wild optimisms to construct surrogates to the true optimism, and then formed approximations to the MSE via equation (5).

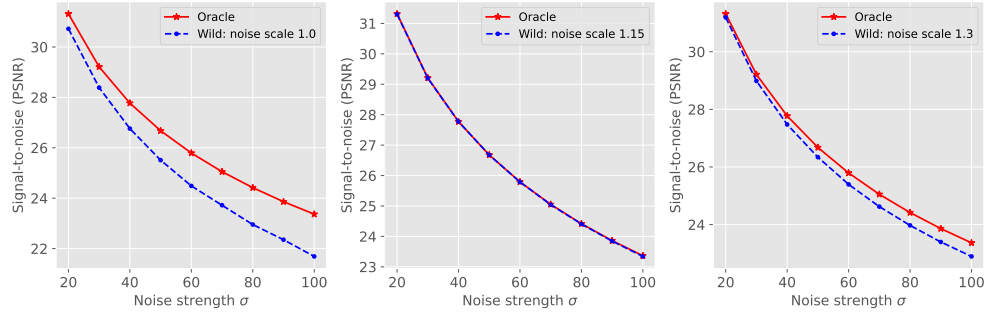
Figure 5 gives plots of the true MSE, along with these three wild-refitting estimates of the MSE, versus the log radius $\log r$ as a parameter. We used the wild-refitted MSE with $\rho = 1.2$ to choose the nuclear norm radius, and the minimum of this curve gives the value $r^* = \exp(5.8) \approx 330$. This choice r^* was used to produce the reconstruction $\widehat{\mathbf{S}}_{r^*}$ in the right-most column of Figure 4.

4.2 Plug-and-play image restoration

We now illustrate the use of wild refitting for MSE estimation for image denoising. The denoising problem is a core challenge in statistical image processing, and has received renewed attention given the central role of denoising in generative image modeling.



(a)



(b)

Figure 6. Performance of wild refitting for MSE estimation for plug-and-play denoising for Gaussian noise. Top plots: Denoised images \hat{f}_γ as the smoothing parameter is decreased from left to right. Panel (a): Plots of the true MSE and wild refitting estimates versus the smoothing parameter. Panel (b): Denoising performance measured in terms of pSNR (higher is better) when wild refitting is used to choose the smoothing parameter γ . The red-diamond solid curve plots the pSNR achieved by the oracle choice versus the true noise standard deviation σ , whereas the blue-circle dashed curve plots the pSNR achieved by wild refitting. Wild refitting with $\rho = 1.15$ yields performance that is identical to the oracle in this particular case.

4.2.1 Set-up

Let us begin by setting up the denoising problem using the notation of this paper. In abstract terms, we can represent an 2D-image as a function $f^* : [0, 1]^2 \rightarrow \mathbb{R}$. The digitized version of the image—one that we would view on a computer—can be thought of as a finite set of function evaluations: fixing some set of covariates $\{x_i\}_{i=1}^n$ contained within the unit square, the digitized image is defined by the function evaluations $\{f^*(x_i)\}_{i=1}^n$. In a typical case, the covariates would form a regular grid pattern on the unit square $[0, 1]^2$.

In a denoising problem, we observe n samples of the form $y_i = f^*(x_i) + w_i$ for some additive noise variables w_i satisfying the noise conditions (11b), and our goal is to recover an accurate estimate \hat{f} of the original image f^* . A broad class of methods are based on solving an optimization problem of the form (2), for a suitably penalty function $\mathcal{P} : \mathcal{F} \rightarrow \mathbb{R}$. Often, the exponentiated quantity $e^{-\mathcal{P}(f)}$ is interpreted (modulo normalization) as a prior over the space of images. In these approaches to image denoising—now known as plug-and-play methods [27, 6, 11, 13]—the function \mathcal{P} (or its gradient $\nabla \mathcal{P}$) is learned from a large image database, typically using deep neural networks. This penalty function is then combined with iterative optimization methods (e.g., proximal gradient, ADMM etc.) so as to solve the underlying optimization problem (2). We refer the reader to Kamilov et al. [14] for a survey overview.

In order to explore the use of wild refitting for plug-and-play denoising, we used a Python implementation of a proximal plug-and-play method due to Hurault et al. [13]. It provides a sequence of penalty functions $\{\mathcal{P}_\gamma, \gamma \geq 0\}$, indexed by the *smoothness parameter* γ (corresponding to noise level used in training the deep net prior). In our experiments, we explore the use of wild refitting to automatically select this tuning parameter so as to minimize the MSE of the resulting reconstruction $\hat{f} \equiv \hat{f}_\gamma$.

Using wild refitting for smoothing parameter selection: In practice, given a noisy image \tilde{y} , we would like an automated way of choosing the bandwidth parameter so that the estimate $\hat{f}_\gamma = \mathcal{M}_\gamma(\tilde{y})$ has smallest MSE. The *oracle choice* is to choose

$$\gamma^* := \arg \min_{\gamma \geq 0} \|\hat{f}_\gamma - f^*\|_n^2. \quad (21a)$$

However, it is not implementable, since the true image f^* is unknown. However, for a suitable choice of ρ , wild refitting gives us an upper bound $B_\rho(\gamma)$ on the MSE $\|\hat{f}_\gamma - f^*\|_n^2$, and so we can attempt to mimic the oracle rule by instead choosing the value

$$\gamma_\rho^\bullet := \arg \min_{\gamma \geq 0} B_\rho(\gamma). \quad (21b)$$

We can then compare the oracle MSE $\|\hat{f}_{\gamma^*} - f^*\|_n^2$ to the MSE $\|\hat{f}_{\gamma_\rho^\bullet} - f^*\|_n^2$ obtained from the wild refitting choice γ_ρ^\bullet .

4.2.2 Results

We performed experiments for various images, and various types of noise, including Gaussian, Student- t noise, and heteroskedastic ensembles. Here we report some representative results for such problems.

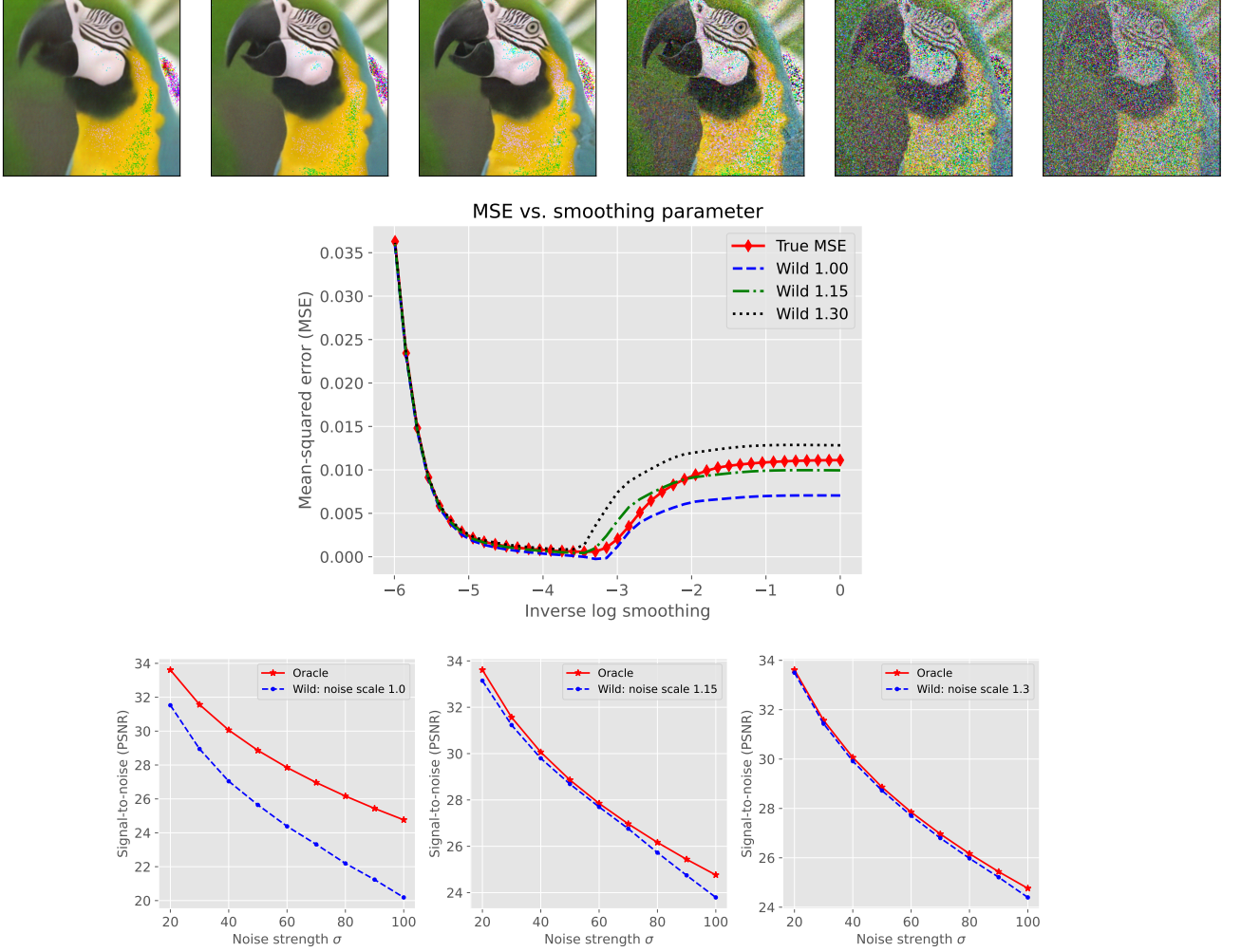


Figure 7. Performance of wild refitting for MSE estimation for plug-and-play denoising with Student- t noise with $d = 6$ degrees of freedom. Top plots: Denoised images \hat{f}_γ as the smoothing parameter is decreased from left to right. Panel (a): Plots of the true MSE and wild refitting estimates versus the smoothing parameter. Panel (b): Denoising performance measured in terms of pSNR (higher is better) when wild refitting is used to choose the smoothing parameter γ . The red-diamond solid curve plots the pSNR achieved by the oracle choice versus the true noise standard deviation σ , whereas the blue-circle dashed curve plots the pSNR achieved by wild refitting. Wild refitting with $\rho = 1.30$ yields the best performance in this case.

Gaussian case: Beginning with the (easiest) case of Gaussian noise, we generated a noisy version of the Sloth image shown in Figure 6 by choosing $w_i \sim N(0, \sigma^2)$. Using this noisy image (represented as a vector $y \in \mathbb{R}^n$, with $n = 512 \times 512$), we then computed the plug-and-play estimate \hat{f}_γ for a range of smoothing parameters γ . In the top row of Figure 6, we plot the denoised images \hat{f}_γ for five different choices of γ , ranging from a larger value (over-smoothed) over to a smaller value (under-smoothed). In panel (a) of Figure 6, we plot the true MSE $\|\hat{f}_\gamma - f^*\|_n^2$ versus the inverse log smoothing parameter $\log(1/\gamma)$, so that the left side (respectively right side) corresponds to

under-smoothing (respectively over-smoothing). We also plot the wild refitting estimates of the MSE for three different choices of the noise scale: $\rho \in \{1.0, 1.15, 1.30\}$. Consistent with our theory, the wild refitting estimates are upper bounds on the true MSE once ρ is sufficiently large; in this example, setting $\rho = 1.15$ is sufficient.

Panel (b) in [Figure 6](#) compares the MSE obtained by the oracle choice γ^* to the MSE obtained by the wild refitting choice γ_ρ^* ; in each case, we plot these MSEs versus the true standard deviation σ of the additive Gaussian noise variables ($w \sim N(0, \sigma^2)$). The left-middle-right panels correspond to the wild noise scales $\rho \in \{1.0, 1.15, 1.30\}$. In this particular case, we see that with the choice $\rho = 1.15$, the MSE obtained from the wild choice γ_ρ^* is *identical* to the oracle MSE.

Student-*t* noise: We then moved onto a more challenging case of heavy-tailed noise, in particular choosing the w_i -variables to have a Student-*t* distribution with $d = 6$ degrees of freedom. Focusing on the Parrot image shown in [Figure 7](#), we again computed the plug-and-play estimate \hat{f}_γ for a range of smoothing parameters γ , and we plot these denoised images in the top row of [Figure 7](#), for five different choices of γ . Panel (a) of [Figure 7](#) gives plots of the true MSE $\|\hat{f}_\gamma - f^*\|_n^2$ and wild refitting estimates of the MSE versus the inverse log smoothing parameter $\log(1/\gamma)$. We plot the wild refitting estimates of the MSE for three different choices of the noise scale: $\rho \in \{1.0, 1.15, 1.30\}$. Consistent with our theory, the wild refitting estimates are upper bounds on the true MSE once ρ is sufficiently large; in this example, setting $\rho = 1.30$ is adequate. It is worth noting that the wild MSE estimate with $\rho = 1.0$ is a severe under-estimate; in fact, the MSE estimate is negative for certain values of γ .

Panel (b) in [Figure 7](#) compares the MSE obtained by the oracle choice γ^* to the MSE obtained by the wild refitting choice γ_ρ^* . Again, we plot these MSEs versus the standard deviation σ of the underlying noise variables (Student-*t* in this case). The left-middle-right panels correspond to the wild noise scales $\rho \in \{1.0, 1.15, 1.30\}$; for this Student-*t* noise, the choice $\rho = 1.30$ yields the best approximation to the oracle MSE.

Highly heteroskedastic noise: As previously discussed, an important feature of wild refitting is that it allows for heteroskedastic noise. Accordingly, for our final set of experiments, we performed denoising when the contaminating noise variables w_i were highly heteroskedastic. As illustrated in the rightmost image in top row of [Figure 8](#), we contaminated the Starfish image with noise that has a very high standard deviation σ_1 in a central band, and a much smaller standard deviation $\sigma_0 \ll \sigma_1$ outside of this central band. We then applied the plug-and-play denoiser to compute denoised images \hat{f}_γ across a range of smoothing levels γ , as shown in the remaining panels. Panel (a) of [Figure 8](#) gives plots of the true MSE $\|\hat{f}_\gamma - f^*\|_n^2$ and wild refitting estimates of the MSE versus the inverse log smoothing parameter $\log(1/\gamma)$. We plot the wild refitting estimates of the MSE for three different choices of the noise scale: $\rho \in \{1.0, 1.15, 1.30\}$. Consistent with our theory, the wild refitting estimates are upper bounds on the true MSE once ρ is sufficiently large; in this example, setting $\rho = 1.30$ is adequate.

Panel (b) in [Figure 8](#) compares the MSE obtained by the oracle choice γ^* to the MSE obtained by the wild refitting choice γ_ρ^* . We plot these MSEs versus the square root of the average variance: that is, the quantity $\sigma := \sqrt{\frac{1}{n} \sum_{i=1} \sigma^2(x_i)}$, where $\sigma^2(x_i)$ is the variance of the noise at image position x_i . The left-middle-right panels correspond to the wild noise scales $\rho \in \{1.0, 1.15, 1.30\}$; Among these three choices, setting $\rho = 1.30$ yields the best approximation to the oracle MSE, but we see that it does not exactly match the oracle in this more challenging case.

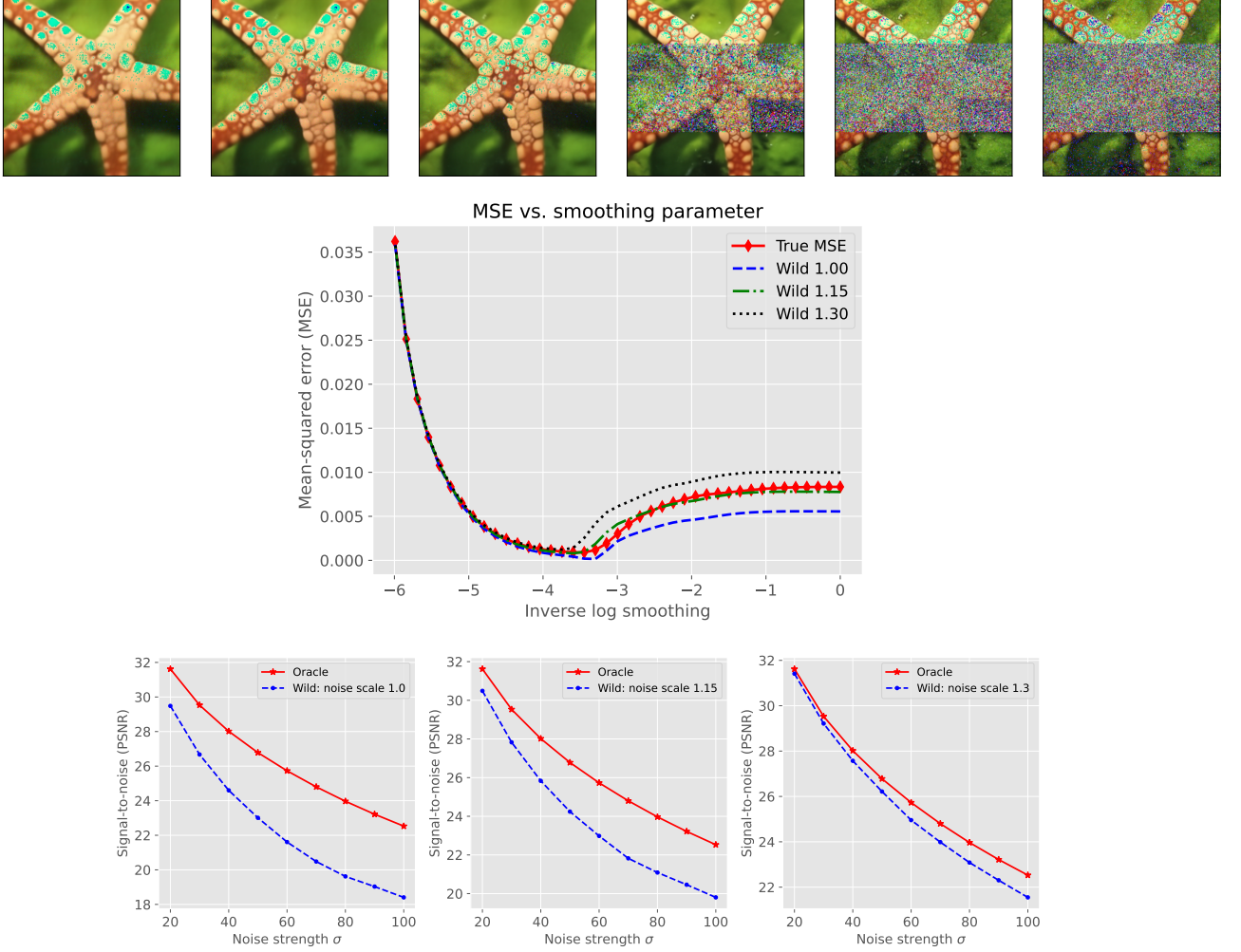


Figure 8. Performance of wild refitting for MSE estimation for plug-and-play denoising with a heterogenous form of noise: the middle strip has high variance, with the outer strips having very low variance. Top plots: Denoised images \hat{f}_γ as the smoothing parameter is decreased from left to right. Panel (a): Plots of the true MSE and wild refitting estimates versus the smoothing parameter. Panel (b): Denoising performance measured in terms of pSNR (higher is better) when wild refitting is used to choose the smoothing parameter γ . The red-diamond solid curve plots the pSNR achieved by the oracle choice versus the true noise standard deviation σ , whereas the blue-circle dashed curve plots the pSNR achieved by wild refitting. Wild refitting with $\rho = 1.30$ yields the best performance among these three choices, but does not match the oracle performance exactly, especially for larger values of σ .

5 Proofs

In this section, we turn to the proofs of our main claims, including [Theorems 1](#) and [2](#) in [Sections 5.1](#) and [5.3](#), respectively.

5.1 Proof of Theorem 1

Our proof involves relating the optimism and its wild variant via the intermediate quantities

$$\text{Opt}^\dagger(\hat{f}) = \frac{1}{n} \sum_{i=1}^n w_i (\hat{f}(x_i) - f^\dagger(x_i)), \quad \text{and} \quad (22a)$$

$$Z_n^\varepsilon(r) := \sup_{f \in \mathbb{B}_r(f^\dagger)} \left[\frac{1}{n} \sum_{i=1}^n \varepsilon_i w_i (f(x_i) - f^\dagger(x_i)) \right]. \quad (22b)$$

The following lemma shows how they can be used to bound the optimism:

Lemma 2. *For any $t > 0$, we have*

$$\text{Opt}^*(\hat{f}) \leq \text{Opt}^\dagger(\hat{f}) + \|f^\dagger - f^*\|_n \frac{2\|w\|_\infty t}{\sqrt{n}} \quad \text{with probability at least } 1 - e^{-t^2}. \quad (23a)$$

Moreover, for any $r \geq \|\hat{f} - f^\dagger\|_n$ and any $t > 0$, we have

$$\max \{ \text{Opt}^\dagger(\hat{f}), Z_n^\varepsilon(r) \} \leq \mathbb{E}_\varepsilon[Z_n^\varepsilon(r)] + r \frac{2\|w\|_\infty t}{\sqrt{n}}. \quad (23b)$$

with probability at least $1 - 2e^{-t^2}$.

See [Section 5.2.1](#) for the proof of this claim.

Based on [Lemma 2](#), we see that for any $r \geq \|\hat{f} - f^\dagger\|_n$, we have the upper bound

$$\text{Opt}^*(\hat{f}) \leq \mathbb{E}_\varepsilon[Z_n^\varepsilon(r)] + \{r + \|f^\dagger - f^*\|_n\} \frac{2\|w\|_\infty t}{\sqrt{n}} \quad (24)$$

with probability at least $1 - 3e^{-t^2}$. Our next step is to relate the expectation $\mathbb{E}_\varepsilon[Z_n^\varepsilon(r)]$ to the wild optimism $\widetilde{\text{Opt}}^\dagger(\hat{f})$. In order to do so, we make use of the intermediate family of random variables

$$W_n^{\text{ideal}}(r) := \sup_{f \in \mathbb{B}_r(\hat{f})} \left[\frac{1}{n} \sum_{i=1}^n \varepsilon_i w_i (f(x_i) - \hat{f}(x_i)) \right]. \quad (25)$$

The following auxiliary result relates the expectations of $Z_n^\varepsilon(r)$ and $W_n^{\text{ideal}}(r)$, and involves the estimation error $\hat{r}_n := \|\hat{f} - f^\dagger\|_n$.

Lemma 3. *We have the deterministic bound*

$$\mathbb{E}_\varepsilon[Z_n^\varepsilon(r)] \leq \mathbb{E}_\varepsilon[W_n^{\text{ideal}}(r + \hat{r}_n)] \quad (26a)$$

along with the bound

$$\mathbb{E}_\varepsilon[W_n^{\text{ideal}}(r)] \leq W_n^{\text{ideal}}(r) + r \frac{2\|w\|_\infty t}{\sqrt{n}} \quad \text{with probability at least } 1 - e^{-t^2}. \quad (26b)$$

See [Section 5.2.2](#) for the proof of this claim.

The two bounds from [Lemma 3](#) imply that for any $r \geq \hat{r}_n$, we have

$$\mathbb{E}_\varepsilon[Z_n^\varepsilon(2r)] \leq W_n^{\text{ideal}}(2r) + (2r) \frac{2\|w\|_\infty t}{\sqrt{n}}$$

with probability at least $1 - e^{-t^2}$. Combined with our earlier inequality (24), we have shown that

$$\text{Opt}^*(\hat{f}) \leq W_n^{\text{ideal}}(2r) + \{3r + \|f^\dagger - f^*\|_n\} \frac{2\|w\|_\infty t}{\sqrt{n}} \quad (27)$$

with probability at least $1 - 4e^{-t^2}$. Our final step is to relate $W_n^{\text{ideal}}(2r)$ to the wild optimism $\widetilde{\text{Opt}}^*(f_\rho^*)$ for a suitably chosen noise scale ρ .

Lemma 4. *For any radius r , we have*

$$W_n^{\text{ideal}}(2r) \leq \widetilde{\text{Opt}}^*(f_\rho^*) + A_n(\tilde{f}), \quad (28)$$

where f_ρ^* is the wild solution with $\|f_\rho^* - \tilde{f}\|_n = 2r$.

See [Section 5.2.3](#) for the proof of this claim.

Finally, by applying the bound (28) to our earlier inequality (27), we find that

$$\text{Opt}^*(\hat{f}) \leq \widetilde{\text{Opt}}^*(f_\rho^*) + \{3r + \|f^\dagger - f^*\|_n\} \frac{2\|w\|_\infty t}{\sqrt{n}} + A_n(\tilde{f}),$$

with probability at least $1 - 4e^{-t^2}$, as claimed in [Theorem 1](#).

5.2 Auxiliary lemmas for [Theorem 1](#)

In this section, we collect together the proofs of the auxiliary lemmas used in the proof of [Theorem 1](#).

5.2.1 Proof of [Lemma 2](#)

We split our analysis into two parts, corresponding to the two claims in the lemma.

Proof of the bound (23a): Beginning with the definition of the optimism (5), we can add and subtract terms involving f^\dagger , thereby obtaining

$$\text{Opt}^*(\hat{f}) = \underbrace{\langle w, \hat{f} - f^\dagger \rangle_n}_{\text{Opt}^\dagger(\hat{f})} + \underbrace{\langle w, f^\dagger - f^* \rangle_n}_T.$$

It remains to bound the term T . Since variable w_i has a distribution symmetric around zero, we can write $w_i = \varepsilon_i |w_i|$, where $\varepsilon_i \in \{-1, +1\}$ is a random sign (Rademacher variable) independent of $|w_i|$. Conditioning on the absolute values, we can represent T as a realization of the linear (and hence convex) function

$$(\varepsilon_1, \dots, \varepsilon_n) \mapsto G(\varepsilon) := \langle \varepsilon |w|, f^\dagger - f^* \rangle_n = \left\{ \frac{1}{n} \sum_{i=1}^n \varepsilon_i |w_i| (f^\dagger(x_i) - f^*(x_i)) \right\}.$$

Letting ε and ε' be two Rademacher sequences, applying the Cauchy–Schwarz inequality yields

$$\begin{aligned} |G(\varepsilon) - G(\varepsilon')| &= \frac{1}{n} \sum_{i=1}^n (\varepsilon_i - \varepsilon'_i) |w_i| (f^\dagger(x_i) - f^*(x_i)) \leq \frac{1}{n} \left(\sum_{i=1}^n w_i^2 (f^\dagger(x_i) - f^*(x_i))^2 \right)^{1/2} \|\varepsilon - \varepsilon'\|_2 \\ &\leq \frac{\|w\|_\infty}{\sqrt{n}} \|f^\dagger - f^*\|_n \|\varepsilon - \varepsilon'\|_2 \end{aligned}$$

showing that the function G is L -Lipschitz with $L := \frac{\|w\|_\infty}{\sqrt{n}} \|f^\dagger - f^*\|_n$. Since $\mathbb{E}_\varepsilon[G(\varepsilon)] = 0$, standard concentration results for convex/Lipschitz functions of Rademacher variables (cf. Theorem 3.24 in the book [28]) guarantee that

$$G(\varepsilon) \leq \frac{2\|w\|_\infty t}{\sqrt{n}} \|f^\dagger - f^*\|_n \quad \text{with probability at least } 1 - e^{-t^2}.$$

Proof of the bound (23b): We condition on the vector $|w|$ of absolute values throughout this proof. Letting $\varepsilon \in \{-1, +1\}^n$ be an i.i.d. vector of Rademacher variables, we can view the random variable $Z_n^\varepsilon(r)$ as a function

$$\varepsilon \mapsto H(\varepsilon) := Z_n^\varepsilon(r) := \sup_{f \in \mathbb{B}_r(f^\dagger)} \left[\frac{1}{n} \sum_{i=1}^n \varepsilon_i |w_i| (f(x_i) - f^\dagger(x_i)) \right].$$

As in our previous proof, we can write $w_i = \tilde{\varepsilon}_i |w_i|$, where $\tilde{\varepsilon}_i \in \{-1, +1\}$ is a Rademacher variable independent of $|w_i|$. Thus, we recognize the random variable $Z_n(r)$ as a particular realization of the random variable defined by H . Consequently, bounding the difference $Z_n(r) - \mathbb{E}_\varepsilon[Z_n^\varepsilon(r)]$ is equivalent to establishing an upper tail bound for $H(\varepsilon)$ in terms of its expectation $\mathbb{E}_\varepsilon[H(\varepsilon)]$. In particular, the claim is equivalent to showing that $H(\varepsilon) \leq \mathbb{E}_\varepsilon[H(\varepsilon)] + r \left(\frac{2\|w\|_\infty t}{\sqrt{n}} \right)$ with probability at least $1 - e^{-t^2}$.

In order to establish this claim, we again make use of concentration bounds for convex and Lipschitz functions of independent bounded random variables (cf. Theorem 3.24 in the book [28]). As a supremum of linear functions, the function H is convex. The claimed bound follows as long as we can establish the Lipschitz bound

$$|H(\varepsilon) - H(\varepsilon')| \leq L \|\varepsilon - \varepsilon'\|_2 \quad \text{for } L = \frac{\|w\|_\infty}{\sqrt{n}} r, \quad (29)$$

valid for any pair of Rademacher vectors $\varepsilon, \varepsilon' \in \{-1, +1\}^n$.

Let g by any function that achieves the supremum defining $H(\varepsilon)$. We can then write

$$\begin{aligned} H(\varepsilon) - H(\varepsilon') &\leq \left[\frac{1}{n} \sum_{i=1}^n \varepsilon_i |w_i| (g(x_i) - f^\dagger(x_i)) \right] - \left[\frac{1}{n} \sum_{i=1}^n \varepsilon'_i |w_i| (g(x_i) - f^\dagger(x_i)) \right] \\ &= \frac{1}{n} \sum_{i=1}^n (\varepsilon_i - \varepsilon'_i) |w_i| (g(x_i) - f^\dagger(x_i)). \end{aligned}$$

Applying the Cauchy–Schwarz inequality yields

$$\begin{aligned} H(\varepsilon) - H(\varepsilon') &\leq \frac{1}{n} \left\{ \sum_{i=1}^n w_i^2 (g(x_i) - f^\dagger(x_i))^2 \right\}^{1/2} (\|\varepsilon - \varepsilon'\|_2) \leq \frac{\|w\|_\infty}{\sqrt{n}} \|g - f^\dagger\|_n \|\varepsilon - \varepsilon'\|_2 \\ &\stackrel{(*)}{\leq} \frac{\|w\|_\infty}{\sqrt{n}} r \|\varepsilon - \varepsilon'\|_2. \end{aligned}$$

where the final bound $(*)$ follows since $\|g - f^\dagger\|_n \leq r$. The same argument applies with the roles of ε and ε' reversed, from which the claimed Lipschitz bound (29) follows.

5.2.2 Proof of Lemma 3

We prove each of the two claims in turn.

Proof of the bound (26a): Let $g \in \mathbb{B}_r(f^\dagger)$ be any function that achieves the supremum defining $Z_n^\varepsilon(r)$. In terms of this function, we have the decomposition $Z_n^\varepsilon(r) = \frac{1}{n} \sum_{i=1}^n \varepsilon_i w_i (g(x_i) - f^\dagger(x_i)) = T_1 + T_2$, where

$$T_1 := \frac{1}{n} \sum_{i=1}^n \varepsilon_i w_i (g(x_i) - \hat{f}(x_i)), \quad \text{and} \quad T_2 := \frac{1}{n} \sum_{i=1}^n \varepsilon_i w_i (\hat{f}(x_i) - f^\dagger(x_i)).$$

By the triangle inequality, we have

$$\|g - \hat{f}\|_n \leq \|g - f^\dagger\|_n + \|f^\dagger - \hat{f}\|_n \leq 2r.$$

where the final step follows since \hat{f} and g belong the ball $\mathbb{B}_r(f^\dagger)$. Consequently, we have shown that

$$T_1 \leq \sup_{f \in \mathbb{B}_{2r}(\hat{f})} \frac{1}{n} \sum_{i=1}^n \varepsilon_i w_i (g(x_i) - \hat{f}(x_i)), \quad \text{and hence} \quad \mathbb{E}_\varepsilon[T_1] \leq \mathbb{E}_\varepsilon[W_n^{\text{ideal}}(2r)].$$

As for the second term, we have

$$\mathbb{E}_\varepsilon[T_2] = \mathbb{E}_\varepsilon \left[\frac{1}{n} \sum_{i=1}^n \varepsilon_i w_i (\hat{f}(x_i) - f^\dagger(x_i)) \right] = 0,$$

using the fact that ε_i is a Rademacher variable independent of the original noise vector w_i , and hence \hat{f} as well. Putting together the pieces, we have shown that

$$\mathbb{E}_\varepsilon[Z_n^\varepsilon(r)] \leq \mathbb{E}_\varepsilon[T_1] = \mathbb{E}_\varepsilon[W_n^{\text{ideal}}(2r)],$$

thus establishing the claim (26a) of Lemma 3.

Proof of the bound (26b): The random variable $W_n^{\text{ideal}}(r)$ has a structure analogous to $Z_n^\varepsilon(r)$, so that this claim follows by an argument entirely analogous to that used to prove the claim (23b) from Lemma 2.

5.2.3 Proof of Lemma 4

By definition of the wild noise $\tilde{w}_i = y_i - \tilde{f}(x_i)$, we have

$$\varepsilon_i w_i = \varepsilon_i \tilde{w}_i + \varepsilon_i (\tilde{f}(x_i) - f^*(x_i)).$$

Consequently, from the definition of W_n^{ideal} combined with the triangle inequality, we can write

$$\begin{aligned} W_n^{\text{ideal}}(2r) &= \sup_{f \in \mathbb{B}_{2r}(\tilde{f})} \left[\frac{1}{n} \sum_{i=1}^n \varepsilon_i w_i (f(x_i) - \tilde{f}(x_i)) \right] \\ &\leq \sup_{f \in \mathbb{B}_{2r}(\tilde{f})} \left[\frac{1}{n} \sum_{i=1}^n \varepsilon_i \tilde{w}_i (f(x_i) - \tilde{f}(x_i)) \right] + \sup_{f \in \mathbb{B}_{2r}(\tilde{f})} \left[\frac{1}{n} \sum_{i=1}^n \varepsilon_i (\tilde{f}(x_i) - f^*(x_i)) (f(x_i) - \tilde{f}(x_i)) \right] \\ &= W_n(2r) + A_n(\tilde{f}). \end{aligned} \tag{30}$$

Finally, by [Lemma 1](#), we have the equivalence $W_n(2r) = \widetilde{\text{Opt}}^\bullet(f_\rho^\bullet)$ for the wild solution f_ρ^\bullet with noise scale ρ chosen to ensure that $\|f_\rho^\bullet - \widehat{f}\|_n = 2\rho$.

5.3 Proof of [Theorem 2](#)

We now turn to the proof of [Theorem 2](#), which provides upper bounds on the estimation error $\widehat{r}_n := \|\widehat{f} - f^\dagger\|_n$.

5.3.1 Proof of the bound (16a)

Our proof of this claim requires two auxiliary results, which we begin by stating.

Lemma 5. *Given a procedure \mathcal{M} that is firmly non-expansive (11a) around f^* , the error $\widehat{r}_n := \|\widehat{f} - f^\dagger\|_n$ satisfies the bound*

$$\widehat{r}_n^2 \leq Z_n(\widehat{r}_n). \quad (31)$$

See [Section 5.4.1](#) for the proof.

We also require the following generalization of the bound (23b) from [Lemma 2](#). In particular, it allows us to bound $Z_n(r)$ for a random radius (such as \widehat{r}_n).

Lemma 6. *For any scalar $s \geq 3$, we have*

$$Z_n(r) \leq \mathbb{E}_\varepsilon [Z_n^\varepsilon([1 + \frac{1}{s}] r)] + \frac{4\|w\|_\infty}{s} r^2 \quad (32)$$

uniformly for all $r \geq \frac{s^2}{\sqrt{n}}$ with probability at least $1 - e^{-s^2}$.

See [Section 5.4.2](#) for the proof.

Equipped with these lemmas, let us now complete the proof of the theorem. Fix some $s \geq 3$. We either have $\widehat{r}_n \leq s^2/\sqrt{n}$, or we may assume that $\widehat{r}_n > s^2/\sqrt{n}$. The remainder of our proof assumes that the latter inequality holds.

We have

$$\widehat{r}_n^2 \stackrel{(i)}{\leq} Z_n(\widehat{r}_n) \stackrel{(ii)}{\leq} \mathbb{E}_\varepsilon [Z_n^\varepsilon([1 + \frac{1}{s}] \widehat{r}_n)] + \frac{4\|w\|_\infty}{s} \widehat{r}_n^2,$$

where step (i) follows from [Lemma 5](#); and inequality (ii) holds with probability at least $1 - e^{-s^2}$, based on [Lemma 6](#). By applying the bound (26a) from [Lemma 3](#) with $r = \widehat{r}_n$, we find that

$$\widehat{r}_n^2 \leq \mathbb{E}_\varepsilon [W_n^{\text{ideal}}([2 + \frac{1}{s}] \widehat{r}_n)] + \frac{4\|w\|_\infty}{s} \widehat{r}_n^2. \quad (33a)$$

Next we apply the bound (26b) from [Lemma 2](#) with the choice $t = \widehat{r}_n \sqrt{n}/s$, thereby obtaining³

$$\mathbb{E}_\varepsilon [W_n^{\text{ideal}}([2 + \frac{1}{s}] \widehat{r}_n)] \leq W_n^{\text{ideal}}([2 + \frac{1}{s}] \widehat{r}_n) + \frac{2\|w\|_\infty}{s} \widehat{r}_n^2, \quad (33b)$$

³To be clear, while \widehat{r}_n is a random radius, this randomness is independent of the Rademacher randomness that defines W_n^{ideal} , so that we do not use a uniform radius result.

with probability at least $1 - e^{-t^2}$. With our choice $t = \hat{r}_n\sqrt{n}/s$, we have $t^2 = \hat{r}_n^2 n/s^2 \geq s^2$ since we have assumed that $\hat{r}_n \geq s^2/\sqrt{n}$ in this portion of the argument; as consequence, the bound (33b) holds with probability at least $1 - e^{-s^2}$.

By combining inequalities (33a) and (33b), with probability at least $1 - 2e^{-s^2}$, we have

$$\hat{r}_n^2 \leq W_n^{\text{ideal}}([2 + \frac{1}{s}]\hat{r}_n) + \frac{4\|w\|_\infty}{s}\hat{r}_n^2 \stackrel{(*)}{\leq} W_n([2 + \frac{1}{s}]\hat{r}_n) + \frac{4\|w\|_\infty}{s}\hat{r}_n^2 + A_n(\tilde{f}),$$

where step $(*)$ follows inequality (30) from the proof of Lemma 4 in Section 5.2.3. (In particular, we use the bound (30) with the choice $r = 1/2([2 + \frac{1}{s}]\hat{r}_n)$.)

Modulo the replacement of s by t , we have thus established the claim (16a) from Theorem 2. (The additional term t^2/n arises from taking into account the possibility that $\hat{r}_n \leq t/\sqrt{n}$ in our argument.)

5.3.2 Proof of the bound (16b)

In order to prove the bound (16b), we require the following auxiliary result.

Lemma 7. *For any convex function class \mathcal{F} , the function $u \mapsto W_n(u)$ is concave on the interval $[0, \infty]$, and hence we have the non-increasing property*

$$\frac{W_n(s)}{s} \leq \frac{W_n(t)}{t} \quad \text{for any } s \geq t > 0. \quad (34)$$

See Section 5.4.3 for the proof.

Let us now prove the stated bound (16b). Either we have $\hat{r}_n \leq r_\rho^\bullet$, or $\hat{r}_n > r_\rho^\bullet$. In the latter case, we can write

$$\begin{aligned} W_n([2 + \frac{1}{t}]\hat{r}_n) &= [2 + \frac{1}{t}]\hat{r}_n \frac{W_n([2 + \frac{1}{t}]\hat{r}_n)}{[2 + \frac{1}{t}]\hat{r}_n} \leq [2 + \frac{1}{t}]\hat{r}_n \frac{W_n([2 + \frac{1}{t}]r_\rho^\bullet)}{[2 + \frac{1}{t}]r_\rho^\bullet} \\ &= \hat{r}_n \frac{W_n([2 + \frac{1}{t}]r_\rho^\bullet)}{r_\rho^\bullet}, \end{aligned}$$

where the inequality follows from equation (34) in Lemma 7. Combining with inequality (16a) from Theorem 2 yields the claim (16b).

5.4 Auxiliary lemmas for Theorem 2

In this section, we collect together proofs of the auxiliary lemmas involved in Theorem 2.

5.4.1 Proof of Lemma 5

To prove this claim, we first observe that by definition $\hat{f} = \mathcal{M}(f^* + w)$ and $f^\dagger = \mathcal{M}(f^*)$. Since the estimator \mathcal{M} is firmly non-expansive around f^* , we have

$$\begin{aligned} \hat{r}_n^2 &= \|\hat{f} - f^\dagger\|_n^2 = \|\mathcal{M}(f^* + w) - \mathcal{M}(f^*)\|_n^2 \leq \langle w, \hat{f} - f^\dagger \rangle_n \\ &= \frac{1}{n} \sum_{i=1}^n w_i (\hat{f}(x_i) - f^\dagger(x_i)) \\ &\stackrel{(\dagger)}{\leq} Z_n(\hat{r}_n), \end{aligned}$$

where inequality (\dagger) follows from the definition of Z_n .

5.4.2 Proof of Lemma 6

For an arbitrary $s > 0$, we apply the bound (23b) with $t := nr/s$ to obtain

$$\mathbb{P}[Z_n(r) \geq \mathbb{E}_\varepsilon[Z_n^\varepsilon(r)] + \frac{2\|w\|_\infty}{s} r^2] \stackrel{(i)}{\leq} e^{-\frac{r^2}{s^2}n} \stackrel{(ii)}{\leq} e^{-s^2}. \quad (35)$$

where the final inequality (ii) follows as long as $r \geq s^2/\sqrt{n}$.

Now let \mathcal{E} be the event the bound (32) is violated for some $r \geq \frac{s^2}{\sqrt{n}}$. Our strategy is to exploit the tail bound (35)(i) to prove that $\mathbb{P}[\mathcal{E}] \leq e^{-s^2}$. In order to do so, we first define the increasing sequence

$$q_0 := \frac{s^2}{\sqrt{n}} \quad \text{and} \quad q_m := (1 + \frac{1}{s})^m q_0 \quad \text{for } m = 1, 2, 3, \dots,$$

and then decompose the event of interest as $\mathcal{E} = \cup_{m=0}^\infty \mathcal{E}_m$, where

$$\mathcal{E}_m := \left\{ \exists r \in [q_m, q_{m+1}) \text{ such that the bound (32) is violated} \right\}.$$

We claim that it suffices to show that

$$\mathbb{P}[\mathcal{E}_m] \leq e^{-\frac{n}{s^2}q_{m+1}^2} \quad \text{for each } m = 0, 1, 2, \dots \quad (36)$$

Taking this inequality as given, we can then apply the union bound to obtain

$$\mathbb{P}[\mathcal{E}] \leq \sum_{m=0}^\infty \mathbb{P}[\mathcal{E}_m] \stackrel{(i)}{\leq} \sum_{m=0}^\infty e^{-\frac{n}{s^2}q_{m+1}^2} \stackrel{(ii)}{\leq} e^{-s^2} \sum_{m=0}^\infty e^{-2(m+1)s} \stackrel{(iii)}{\leq} e^{-s^2},$$

where step (i) follows from the bound (36). In order to verify inequality (ii), we observe that

$$\begin{aligned} \frac{n}{s^2} q_{m+1}^2 &= \frac{n}{s^2} (1 + \frac{1}{s})^{2(m+1)} q_0^2 \geq \frac{n}{s^2} q_0^2 \{1 + 2(m+1)(1/s)\} \\ &= s^2 + 2(m+1)s, \end{aligned}$$

using the fact that $(1 + (1/s))^{2(m+1)} \geq 1 + 2(m+1)(1/s)$, and the equality $\frac{n}{s^2} q_0^2 = s^2$. Finally, step (iii) follows since $\sum_{m=0}^\infty e^{-2(m+1)s} \leq \sum_{m=1}^\infty (1/2)^m = 1$, since the assumption that $s \geq 3$ implies that $e^{-2s} \leq \frac{1}{2}$.

Proof of the bound (36): So as to reduce clutter, introduce the shorthand $\bar{Z}_n(r) := \mathbb{E}_\varepsilon[Z_n^\varepsilon(r)]$. If the event \mathcal{E}_m holds, then we are guaranteed to have some $r \in [q_m, q_{m+1}]$ such that

$$\begin{aligned} Z_n(q_{m+1}) &\stackrel{(i)}{\geq} Z_n(r) \stackrel{(ii)}{\geq} \bar{Z}_n([1 + \frac{1}{s}]r) + \frac{4\|w\|_\infty}{s} r^2 \\ &\stackrel{(iii)}{\geq} \bar{Z}_n(q_{m+1}) + \frac{4\|w\|_\infty}{s} q_m^2 \\ &\stackrel{(iv)}{\geq} \bar{Z}_n(q_{m+1}) + \frac{2\|w\|_\infty}{s} q_{m+1}^2, \end{aligned}$$

where step (i) follows since $q_{m+1} \geq r$ and the function $u \mapsto Z_n(u)$ is non-decreasing in u ; inequality (ii) follows by definition of the event \mathcal{E}_m ; inequality (iii) holds since $r \geq q_m$ and $[1 + \frac{1}{s}]r \geq [1 + \frac{1}{s}]q_m = q_{m+1}$; and step (iv) follows since

$$\frac{q_m^2}{q_{m+1}^2} = \frac{1}{[1 + \frac{1}{s}]^2} \geq \frac{1}{(1 + \frac{1}{3})^2} = \frac{9}{16} \geq \frac{1}{2}$$

using the assumption $s \geq 3$.

From this string of inequalities, we can conclude that

$$\mathbb{P}[\mathcal{E}_m] \leq \mathbb{P}\left[Z_n(q_{m+1}) \geq \bar{Z}_n(q_{m+1}) + \frac{2\|w\|_\infty}{s} q_{m+1}^2\right] \stackrel{(v)}{\leq} e^{-\frac{n}{s^2} q_{m+1}^2},$$

where inequality (v) follows by applying the bound (35)(i) with $r = q_{m+1}$. This completes the proof of the auxiliary claim (36), and hence the overall proof.

5.4.3 Proof of Lemma 7

Since $W_n(0) = 0$, the inequality (34) is equivalent to

$$\frac{W_n(s) - W_n(0)}{s} \leq \frac{W_n(t) - W_n(0)}{t} \quad \text{for all } s \geq t > 0.$$

It is a standard fact from convex analysis [20] that any concave function has this property.

Thus, it remains to show that W_n is a concave function: more precisely, we will show that any scalars $s, t \geq 0$ and $\alpha \in [0, 1]$, we have

$$\alpha W_n(s) + (1 - \alpha) W_n(t) \leq W_n(r) \quad \text{where } r := \alpha s + (1 - \alpha)t.$$

Let f_s and f_t be functions achieving the suprema that define $W_n(s)$ and $W_n(t)$, respectively, and introduce the shorthand $f_r = \alpha f_s + (1 - \alpha) f_t$. By the assumed convexity of \mathcal{F} , we have $f_r \in \mathcal{F}$, and moreover, by the triangle inequality, we have

$$\|f_r - \hat{f}\|_n \leq \alpha \|f_s - \hat{f}\|_n + (1 - \alpha) \|f_t - \hat{f}\|_n \leq \alpha s + (1 - \alpha)t = r.$$

Consequently, the function f_α is feasible for the supremum defining $W_n(r)$, so that we can write

$$\begin{aligned} \alpha W_n(s) + (1 - \alpha) W_n(t) &= \frac{1}{n} \sum_{i=1}^n \varepsilon_i \tilde{w}_i (\alpha f_s(x_i) + (1 - \alpha) f_t(x_i) - \hat{f}(x_i)) \\ &\leq \sup_{f \in \mathbb{B}_{\hat{f}}(r)} \frac{1}{n} \sum_{i=1}^n \varepsilon_i \tilde{w}_i (f(x_i) - \hat{f}(x_i)) = W_n(r), \end{aligned}$$

as claimed.

6 Discussion

{GD: To do}

In this paper, we

Acknowledgements

This work was partially supported by the Cecil H. Green Chair, ONR grant N00014-21-1-2842 from the Office of Naval Research, and NSF DMS-2311072 from the National Science Foundation. It was inspired by interactions with Peter Bühlmann at the Oberwolfach Research Institute, along with repeated in-person demonstrations of his dancing skills.

7 Proof of Lemma 1

In this lemma statement, the penalty function \mathcal{P} is the indicator for membership in the convex set \mathcal{C} . With a slight abuse of notation, we write $f \in \mathcal{C}$ as a shorthand for $(f(x_1), \dots, f(x_n)) \in \mathcal{C}$. By definition, the wild estimate f_ρ^\bullet is a constrained minimizer of the objective

$$\arg \min_{f \in \mathcal{C}} \left\{ \frac{1}{2n} \sum_{i=1}^n (y_i^\bullet - f(x_i))^2 \right\} = \arg \min_{f \in \mathcal{C}} \left\{ \frac{1}{2} \|f - \hat{f}\|_n^2 - \rho \frac{1}{n} \sum_{i=1}^n \varepsilon_i \tilde{w}_i (f(x_i) - \hat{f}(x_i)) \right\}.$$

Equivalently, for each radius $r \geq 0$, define the shell $\mathcal{C}(r) = \{f \in \mathcal{C} \mid \|f - \hat{f}\|_n = r\}$. We then write

$$\begin{aligned} \min_{f \in \mathcal{C}} \left\{ \frac{1}{2} \|f - \hat{f}\|_n^2 - \rho \frac{1}{n} \sum_{i=1}^n \varepsilon_i \tilde{w}_i (f(x_i) - \hat{f}(x_i)) \right\} &= \min_{r \geq 0} \min_{f \in \mathcal{C}(r)} \left\{ \frac{r^2}{2} - \rho \frac{1}{n} \sum_{i=1}^n \varepsilon_i \tilde{w}_i (f(x_i) - \hat{f}(x_i)) \right\} \\ &= \min_{r \geq 0} \left\{ \frac{r^2}{2} - \rho W_n(r) \right\}, \end{aligned}$$

using the definition of the wild complexity.

The left-hand side is minimized at f_ρ^\bullet whereas the right-hand side is minimized at $r_\rho^\bullet = \|f_\rho^\bullet - \hat{f}\|_n$. Evaluating the left-hand side at f_ρ^\bullet yields

$$\frac{1}{2} \|f_\rho^\bullet - \hat{f}\|_n^2 - \rho \frac{1}{n} \sum_{i=1}^n \varepsilon_i \tilde{w}_i (f_\rho^\bullet(x_i) - \hat{f}(x_i)) = \frac{(r_\rho^\bullet)^2}{2} - \rho \widetilde{\text{Opt}}^\bullet(f_\rho^\bullet)$$

Evaluating the right-hand side at r_ρ^\bullet yields

$$\frac{(r_\rho^\bullet)^2}{2} - \rho W_n(r_\rho^\bullet) = \frac{(r_\rho^\bullet)^2}{2} - W_n(\|f_\rho^\bullet - \hat{f}\|_n),$$

and by comparing these expressions, we see that $W_n(r_\rho^\bullet) = \widetilde{\text{Opt}}^\bullet(f_\rho^\bullet)$ for any $\rho > 0$, as claimed.

References

- [1] I. Akhter, Y. Sheikh, S. Khan, and T. Kanade. Trajectory space: A dual representation of nonrigid structure from motion. *IEEE Trans. PAMI*, 33(7):1442–1456, 2011.
- [2] S. Arlot and A. Celisse. A survey of cross-validation procedures for model selection. *Statistics Surveys*, 4:40–79, 2010.
- [3] S. Bates, T. Hastie, and R. Tibshirani. Cross-validation: What does it estimate and how well does it do it? *Journal of the American Statistical Association*, 119(546):1434–1445, 2024.
- [4] C. Bregler, A. Hertzmann, and H. Biermann. Recovering non-rigid 3d shape from image streams. In *Proceedings of the IEEE Conference on Computer Vision and Pattern Recognition (CVPR)*, pages 690–696, 2000.
- [5] Carnegie Mellon University. Cmu graphics lab motion capture database. <http://mocap.cs.cmu.edu/>, 2003.

- [6] S. H. Chan, X. Wang, and O. A. Elgendy. Plug-and-play admm for image restoration: Fixed-point convergence and applications. *IEEE Transactions on Computational Imaging*, 3(1):84–98, 2016.
- [7] Y. Dai, H. Li, and M. He. A simple prior-free method for non-rigid structure-from-motion factorization. *International Journal of Computer Vision*, 107(2):101–122, 2014.
- [8] B. Efron. The estimation of prediction error: Covariance penalties and cross-validation. *Journal of the American Statistical Association*, 99(467):619–632, 2004.
- [9] B. Efron and R. J. Tibshirani. *An Introduction to the Bootstrap*. Chapman & Hall/CRC, New York, 1993.
- [10] S. Geisser. The predictive sample reuse method with applications. *Journal of the American Statistical Association*, 70(350):320–328, 1975.
- [11] A. Graikos, V. Papyan, and J. Mairal. Diffusion models as plug-and-play priors. In *Advances in Neural Information Processing Systems*, volume 35, pages 29213–29226, 2022.
- [12] J. Hiriart-Urruty and C. Lemaréchal. *Fundamentals of convex analysis*. Springer-Verlag, New York, 2001.
- [13] S. Hurault, A. Leclaire, and N. Papadakis. Proximal denoiser for convergent plug-and-play optimization with nonconvex regularization. In *Proceedings of the 39th International Conference on Machine Learning*, pages 9483–9505. PMLR, 2022.
- [14] U. S. Kamilov, C. A. Bouman, G. T. Buzzard, and B. Wohlberg. Plug-and-play methods for integrating physical and learned models in computational imaging. *IEEE Signal Processing Magazine*, 40(1):85–97, 2023.
- [15] M. Ledoux. *The Concentration of Measure Phenomenon*. Mathematical Surveys and Monographs. American Mathematical Society, Providence, RI, 2001.
- [16] K.-C. Li. Resampling residuals: Bootstrap methods for regression models. *Journal of the American Statistical Association*, 84(406):881–889, 1989.
- [17] R. Y. Liu. Bootstrap procedures under some non-i.i.d. models. *Annals of Statistics*, 16(4):1696–1708, 1988.
- [18] E. Mammen. Bootstrap and wild bootstrap for high dimensional linear models. *Annals of Statistics*, 21(1):255–285, 1993.
- [19] Enno Mammen. Bootstrap, wild bootstrap, and asymptotic normality. *Probability Theory and Related Fields*, 93(4):439–455, 1992.
- [20] R. T. Rockafellar. *Convex Analysis*. Princeton University Press, Princeton, 1970.
- [21] R.T. Rockafellar and R. J-B Wets. *Variational Analysis*, volume 317. Springer Science & Business Media, 2009.
- [22] C. Stein. Estimation of the mean of a multivariate normal distribution. *Annals of Statistics*, 9(6):1135–1151, 1981.

- [23] M. Stone. Cross-validatory choice and assessment of statistical predictions. *Journal of the Royal Statistical Society. Series B*, 36(2):111–147, 1974.
- [24] R. Tibshirani and R. J. Tibshirani. A bias correction for the minimum error rate in cross-validation. *Annals of Applied Statistics*, 3(2):822–829, 2009.
- [25] S. van de Geer. *Empirical Processes in M-Estimation*. Cambridge University Press, 2000.
- [26] A. W. van der Vaart and J. Wellner. *Weak Convergence and Empirical Processes*. Springer-Verlag, New York, NY, 1996.
- [27] S. V. Venkatakrishnan, C. A. Bouman, and B. Wohlberg. Plug-and-play priors for model based reconstruction. In *2013 IEEE Global Conference on Signal and Information Processing*, pages 945–948. IEEE, 2013.
- [28] M. J. Wainwright. *High-dimensional statistics: A non-asymptotic viewpoint*. Cambridge University Press, Cambridge, UK, 2019.
- [29] C. F. J. Wu. Jackknife, bootstrap and other resampling methods in regression analysis. *Annals of Statistics*, 14(4):1261–1295, 1986.
- [30] Y. Yang, M. Pilanci, and M. J. Wainwright. Randomized sketches for kernels: Fast and optimal non-parametric regression. *Annals of Statistics*, 45(3):991–1023, 2017.